Solar Radiation Research Laboratory (SRRL) Final Report: Fiscal Years 2019–2021

Manajit Sengupta,[1] Aron Habte,[1] Yu Xie,[1] Peter Gotseff,[1] Mark Kutchenreiter,[1] Afshin Andreas,[1] Ibrahim Reda,[1] Frank Vignola,[2] Anton Driesse,[3] Christian Gueymard,[4] Soutir Bandyopadhyay,[5] and Alexis Denhard[5]

1 National Renewable Energy Laboratory
2 University of Oregon
3 PV Performance Labs
4 Solar Consulting Services
5 Colorado School of Mines

NREL is a national laboratory of the U.S. Department of Energy
Office of Energy Efficiency & Renewable Energy
Operated by the Alliance for Sustainable Energy, LLC

This report is available at no cost from the National Renewable Energy Laboratory (NREL) at www.nrel.gov/publications.

Contract No. DE-AC36-08GO28308

Technical Report
NREL/TP-5D00-81790
Revised May 2022

Solar Radiation Research Laboratory (SRRL) Final Report: Fiscal Years 2019–2021

Manajit Sengupta,[1] Aron Habte,[1] Yu Xie,[1] Peter Gotseff,[1] Mark Kutchenreiter,[1] Afshin Andreas,[1] Ibrahim Reda,[1] Frank Vignola,[2] Anton Driesse,[3] Christian Gueymard,[4] Soutir Bandyopadhyay,[5] and Alexis Denhard[5]

1 National Renewable Energy Laboratory
2 University of Oregon
3 PV Performance Labs
4 Solar Consulting Services
5 Colorado School of Mines

Suggested Citation
Sengupta, Manajit, Aron Habte, Yu Xie, Peter Gotseff, Mark Kutchenreiter, Afshin Andreas, Ibrahim Reda, Frank Vignola, Anton Driesse, Christian Gueymard, Soutir Bandyopadhyay, and Alexis Denhard. 2022. *Solar Radiation Research Laboratory (SRRL) Final Report: Fiscal Years 2019–2021*. Golden, CO: National Renewable Energy Laboratory. NREL/TP-5D00-81790. https://www.nrel.gov/docs/fy22osti/81790.pdf.

NREL is a national laboratory of the U.S. Department of Energy
Office of Energy Efficiency & Renewable Energy
Operated by the Alliance for Sustainable Energy, LLC

This report is available at no cost from the National Renewable Energy Laboratory (NREL) at www.nrel.gov/publications.

Contract No. DE-AC36-08GO28308

Technical Report
NREL/TP-5D00-81790
Revised May 2022

National Renewable Energy Laboratory
15013 Denver West Parkway
Golden, CO 80401
303-275-3000 • www.nrel.gov

NOTICE

This work was authored in part by the National Renewable Energy Laboratory, operated by Alliance for Sustainable Energy, LLC, for the U.S. Department of Energy (DOE) under Contract No. DE-AC36-08GO28308. Funding provided by U.S. Department of Energy Office of Energy Efficiency and Renewable Energy Solar Energy Technologies Office. The views expressed herein do not necessarily represent the views of the DOE or the U.S. Government.

This report is available at no cost from the National Renewable Energy Laboratory (NREL) at www.nrel.gov/publications.

U.S. Department of Energy (DOE) reports produced after 1991 and a growing number of pre-1991 documents are available free via www.OSTI.gov.

Cover Photos by Dennis Schroeder: (clockwise, left to right) NREL 51934, NREL 45897, NREL 42160, NREL 45891, NREL 48097, NREL 46526.

NREL prints on paper that contains recycled content.

Errata

This report, originally published in February 2022, was revised in May 2022 to include a new section about the path forward and a few editorial changes for clarity.

Acknowledgments

We are grateful to the U.S. Department of Energy Office of Energy Efficiency and Renewable Energy Solar Energy Technologies Office and to the Systems Integration and Photovoltaic subprograms for supporting this project. Specifically, we acknowledge Dr. Tassos Golnas, Dr. Guohui Yuan, and Dr. Lenny Tinker for their support and encouragement.

List of Acronyms

ACP	absolute cavity pyrgeometer
APE	absolute percentage error
ARIMA	autoregressive integrated moving average
BMS	Baseline Measurement System
BORCAL	Broadband Outdoor Radiometer Calibration
CRADA	cooperative research and development agreement
DHI	diffuse horizontal irradiance
DISC	Direct Insolation Simulation Code
DISORT	Discrete Ordinates Radiative Transfer
DNI	direct normal irradiance
DOE	U.S. Department of Energy
FARMS-NIT	Fast All-Sky Radiation Model for Solar Applications with Narrowband Irradiances on Tilted Surfaces
GHI	global horizontal irradiance
IEA	International Energy Agency's
IEC	International Electrotechincal Commission
IPC	International Pyrheliometer Comparison
ISO	International Organization for Standardization
LSTM	long short-term memory network
MAE	mean absolute bias error
MAPE	mean absolute percentage error
MBE	mean bias error
MIDC	Measurement and Instrumentation Data Center
NIST	National Institute of Standards and Technology
NPC	National Renewable Energy Laboratory Pyrheliometer Comparisons
NREL	National Renewable Energy Laboratory
NSRDB	National Solar Radiation Database
PACES	Power and Chemical Energy Systems
POA	plane of array
PV	photovoltaic
PVPS	Photovoltaic Power Systems Programme
R&D	research and development
RMSE	root mean square error
SAM	System Advisor Model
SETO	Solar Energy Technologies Office
SMARTS	Simple Model of the Atmospheric Radiative Transfer of Sunshine
SRRL	Solar Radiation Research Laboratory
SURFRAD	Surface Radiation Budget Network
WPVS	World Photovoltaic Scale
WRDC	World Radiation Data Center
WRR	World Radiation Reference

Executive Summary

The Solar Radiation Research Laboratory (SRRL) at the National Renewable Energy Laboratory (NREL) is a world-leading solar calibration and measurement facility and maintains and disseminates the World Radiation Reference (essentially the W/m^2) for the United States, which is essential for traceable and accurate measurements of solar radiation at all solar generation facilities. The NREL-SRRL operates two International Organization for Standardization (ISO)/International Electrotechincal Commission (IEC) 17025 calibration facilities that provide unique, high-quality calibrations to NREL and other U.S. Department of Energy laboratories. The Baseline Measurement System at the NREL-SRRL provides a high-quality record of solar irradiance and surface meteorological conditions. NREL-SRRL capabilities are used to develop (1) improved methods for the calibration of solar radiometers; (2) new standards through the ISO, the IEC, and ASTM International; and (3) models and (4) advanced instrumentation and methods for operating solar measurement stations. The NREL-SRRL data sets are also critical for the validation of new models and data sets, such as the National Solar Radiation Database (NSRDB). This agreement has three tasks that conduct research on advancing solar resource measurements:

- Task 1: Applied solar radiation measurements
- Task 2: Standards development and knowledge sharing
- Task 3: Reference cell calibrations and spectral measurement and modeling for photovoltaic applications.

Table of Contents

List of Figures

List of Tables

1 Background

The primary objective of this project is to reduce risk to solar energy projects by continued the development of established core functions at the National Renewable Energy Laboratory (NREL) addressing solar instrument calibration, resource characterization, and resource data dissemination in support of foundational solar energy research and applications to increase the accuracy of solar resource data, thereby reducing the risks to solar energy projects. Recognizing the needs for improved solar resource measurements, NREL established the Solar Radiation Research Laboratory (SRRL) in 1981 to provide a continuous record of solar irradiance and surface meteorological conditions, improved methods for instrument calibration of spectroradiometers, and the development of advanced instrumentation and methods for operating solar measurement stations.

The NREL-SRRL is located on the top of South Table Mountain on the north side of NREL's South Table Mountain Campus in Golden, Colorado (Figure 1), which has excellent solar access because of the unrestricted view of the sky throughout the year. The NREL-SRRL is home to the world's largest collection of radiometers in continuous operation.

NREL-SRRL (Figure 1) is a unique, world-class research facility that serves as a living laboratory for:

- Solar resource measurement and calibration research and development (R&D)
- The characterization of photovoltaic reference cells.
- The development of standards and best practices for data dissemination.

NREL-SRRL activities allows traceable solar measurements throughout the United States that are essential for project feasibility, due diligence, financing, and plant operations. The NREL-SRRL conducts calibrations on a range of solar resource and other measurement equipment. This report discusses the applied solar radiation measurement research activities that occurred at the NREL-SRRL from fiscal years 2019–2021. Researchers at the NREL-SRRL conduct R&D in applied solar radiation measurements for solar resource assessments and operate a suite of instruments for solar irradiance and meteorological measurements and solar-specific instrument calibrations. Solar resource assessment research activities related to solar instrumentation and measurements at the NREL-SRRL are funded primarily by the U.S. Department of Energy (DOE) Office of Energy Efficiency and Renewable Energy Solar Energy Technologies Office (SETO) Systems Integration program. More details can also be found in the report *Solar Resource Calibration, Measurement, and Dissemination: Final Report FY 2016–FY 2018*.[1]

The R&D conducted at the NREL-SRRL is used to develop international standards such as ASTM standards that reduce business costs for the solar industry. NREL leads the ASTM Subcommittee G03.09 on Radiometry, which is under the ASTM Committee G03: Weathering and Durability; and leads the International Organization for Standardization (ISO)/TC 180/SC 1 Climate – Measurement and Data. Moreover, NREL leads the U.S. effort in the International Energy Agency's (IEA's) Photovoltaic Power Systems Programme (PVPS) Task 16 on Solar Resource for High Penetrations and Large-Scale Applications. NREL also performs the duties of

[1] See https://www.nrel.gov/docs/fy19osti/73667.pdf.

deputy operating agent and assists the operating agent in the administration and reporting that is required by the executive committee of which DOE is a part. Further, NREL, in collaboration with IEA PVPS Task 16, led the update of the third edition of the *Best Practices Handbook for the Collection and Use of Solar Resource Data for Solar Energy Applications*, which is widely used by the solar industry.[2]

The NREL Pyrheliometer Comparisons (NPC) disseminate the World Radiation Reference (WRR), certifying that all complying calibrated solar radiometers in the United States are traceable to the world standard and therefore meet the required standard. The best practices developed through this project enable the solar industry to deploy and measure solar radiation with the highest accuracy and therefore reduce the development costs of the development of solar projects. This project also enables the integration of high penetrations of renewables into the electric grid by providing foundational data sets in support of grid integration. Further, the data are used by technical and economic renewable energy models.

Figure 1. Aerial view of NREL's mesa top facility.

The building in the foreground is the NREL-SRRL. The BMS is mostly deployed on the raised deck to the left (west). *Photo by Dennis Schroeder, NREL*

[2] See https://www.nrel.gov/docs/fy21osti/77635.pdf.

2 Objective

The project sought to use the NREL-SRRL's facilities to enable SETO to achieve its cost targets and enable the large-scale integration of solar energy on the electric grid by reducing the costs and uncertainty in resource measurements through:

- Increased ease of access to the updated world reference to provide traceable calibrations nationwide
- Improved calibration methods for solar radiometers to enhance measurement accuracy
- Providing access to high-quality data sets from various locations for standards and model development and for the evaluation of models and methods
- The development and dissemination of best practices to facilitate high-quality measurements
- The development of standards and best practices in solar measurement and modeling to reduce deployment costs
- Enabling the development of new low-cost, high-quality measurement systems to reduce deployment costs, and
- Collaboration with national and international experts to develop and disseminate innovative methods to improve solar resource assessments.

Provided calibration and characterization of broadband and spectral calibrations and measurements traceable to the WRR in compliance with ISO/International Electrotechnical Commission (IEC) 17025 accreditation requirements.

This involved the operation and maintenance of the Baseline Measurement System (BMS) to provide high-quality, long-term solar and atmospheric measurements. We maintained the national standard for solar measurements and disseminate accurate solar measurement and modeling methods and best practices to various stakeholders, including academia, industry, and laboratories.

This task ensured that relevant instruments are:

- Deployed and maintained following best measurement practices through the BMS
- Calibrated on an annual basis in ISO/IEC 17025-accredited facilities through using the Broadband Outdoor Radiometer Calibration (BORCAL) facility or the Spectral Calibration Laboratory
- Traceable to the WRR through mechanisms such as the NPC.

This task also ensured that data are collected, quality-controlled, and disseminated in a timely manner through the Measurement and Instrumentation Data Center (MIDC). Measurements at the NREL-SRRL were supported by existing infrastructure, which includes maintenance protocols and a budget for equipment replacement costs.

Solar radiation data from across the United States were also collected in collaboration with academic and other research institutions and made public (where allowed by agreements) through the MIDC in real time. Cooperative research-and-development agreements (CRADAs) are used to enable collaboration with instrument manufacturers to evaluate newly developed instruments, thereby supported the advancement of high-quality solar resource measurements.

Provided leadership to develop new standards and update existing standards within ASTM and ISO.

Through this task, we provided leadership within IEA PVPS Task 16, participate in collaborative research, and led the development of the third edition of the *Best Practices Handbook for the Collection and Use of Solar Resource Data for Solar Energy Applications* to include new R&D results in the intervening three years, including work done through the IEA collaboration. We participated in SolarPACES (Power and Chemical Energy Systems) as a U.S. representative for the solar resource and forecasting. Through this task, knowledge generated through from R&D was disseminated to stakeholders.

This task sought to reduce the cost of solar deployment and integration by developing standards for solar measurements and modeling and by summarizing and disseminating information to facilitate the use of new technology by stakeholder. This work was specifically conducted by:

- Providing leadership and developing or updating new standards directly related to solar radiation measurements and modeling under the ASTM G03 (Weathering and Durability) and E44 (Solar, Geothermal, and Other Alternative Energy Sources) committees
- Actively participating in the development of ISO and IEC standards, including acting as liaison between ASTM and ISO
- Performing the duties of deputy operating agent for IEA PVPS Task 16 and participating in collaborative research
- Developing, in collaboration with the experts in IEA PVPS Task 16, the updated third edition of the solar resource measurement, modeling, and forecasting handbook to reflect the current state of knowledge.

Developed methods and models to reduce the uncertainty in the evaluation and prediction of photovoltaic (PV) performance.

As uncertainty in estimating the production of PV plants that are in the development stage leads to enhanced financing cost, this task strived to reduce such costs through reducing uncertainty in PV prediction. In addition, operational PV plants need to meet performance guarantees, and a reduction in the uncertainty in such evaluations, which also leads to a reduction in financing and operation-and-maintenance costs. This task also seeks to reduce the uncertainty in PV performance assessments. Specifically, this task:

- Developed methods to expand the validity of calibrations through developing new methods/processes similar to those used for NREL's ISO-accredited BORCAL process that considers all angles of incidence
- Developed and maintained capabilities to measure spectral radiation at multiple locations using one-axis tracking for use in the validation of spectral data sets generated through the National Solar Radiation Database (NSRDB)
- Maintained and enhanced the capabilities of the NSRDB to provide spectral data sets in the plane of array (POA) on demand
- Developed standard spectra for various standard atmospheres.

3 Project Results and Discussion

3.1 Task 1: Applied Solar Radiation and Measurement

The work performed under this task was divided into two subtasks:

1. Calibration and measurement
2. Dissemination of data and models.

3.1.1 Calibration and Measurement

The following work was performed under this subtask.

3.1.1.1 National and International Pyrheliometer Comparison

The NREL team served as DOE's lead laboratory for radiometer calibration traceable to the WRR (Fröhlich 1991), essential for accurate measurements. Working with the World Radiation Center in Davos, Switzerland, the NREL team participates in the quinquennial International Pyrheliometer Comparisons (IPCs) to maintain the WRR. In turn, annual NPCs provide stakeholders with access to the WRR. For example, NREL published the results of the NPC in 2018 as a technical report,[3] and Figure 2 shows the results of the NREL transfer absolute cavity radiometers. NREL has developed and maintained a select group of absolute cavity radiometers with direct calibration traceability to the WRR (Reda et al. 2019). These instruments are used by NREL to transfer WRR calibrations to other radiometers used and owned by industry. During the NPC, representatives from many national and international agencies participate to maintain radiometer calibration traceability to the WRR. During the 2019 event, 39 participants from 25 organizations around the world came to NREL's South Table Mountain campus to ensure that their 47 absolute cavity radiometers—used to measure direct-beam solar irradiance—are properly calibrated. In 2020, the NREL team planned to participate in the quinquennial IPC, IPC-XIII, to maintain the WRR; however, the IPC-XIII was rescheduled from the original date in 2020 to 2021 due to the COVID-19 pandemic. The Physikalisch-Meteorologisches Observatorium Davos World Radiation Center in Davos, Switzerland, hosts an IPC for transferring the WRR to participating radiometers. Representing DOE, NREL-SRRL staff participated in the IPC-XIII from September 27, 2021–October 15, 2021. The results and report will be published in FY 2022. Note: Because of this rescheduling of the IPC-XIII, NREL did not hold the NPC in 2021.

[3] See https://www.nrel.gov/docs/fy19osti/72607.pdf.

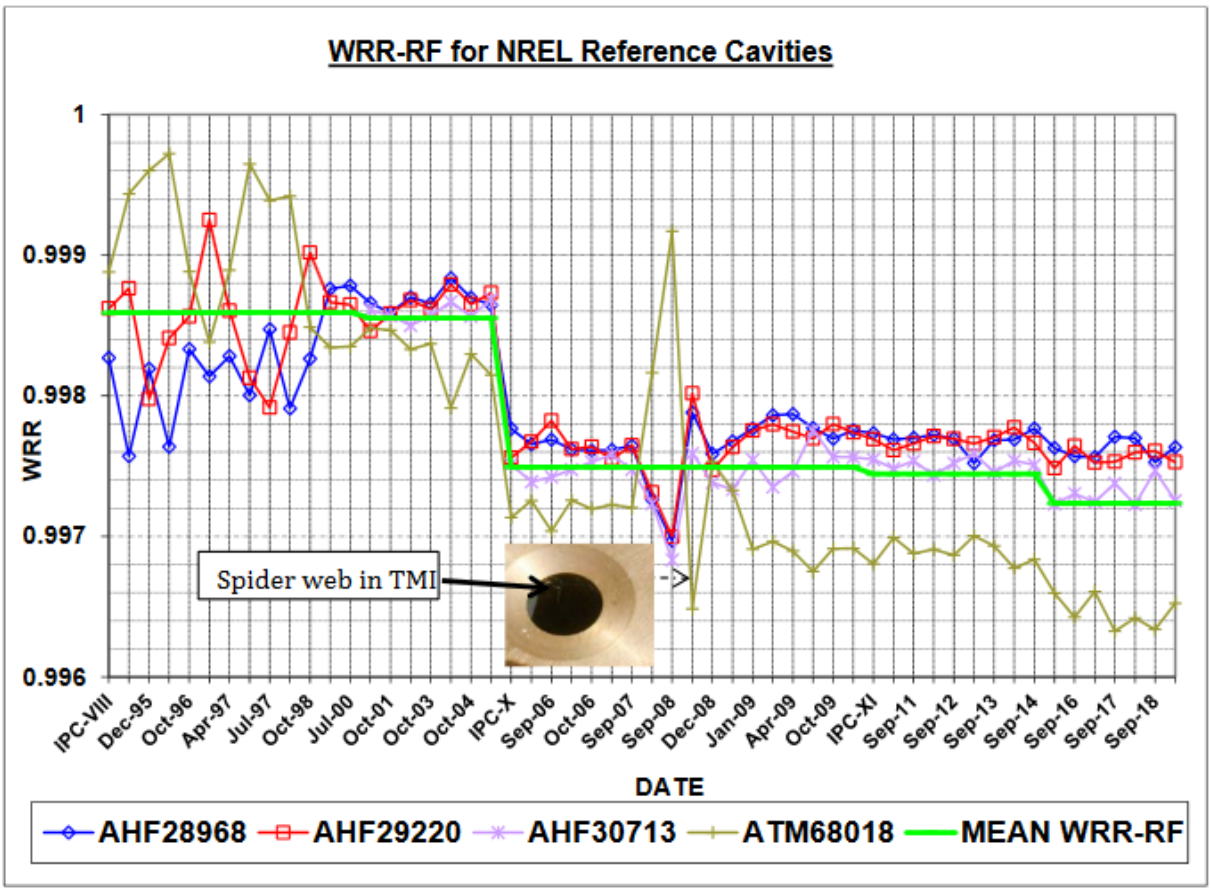

Source: Reda et al. 2019

Figure 2. History of WRR reduction factors for NREL reference cavities. Note: During the NPC of 2008, an abrupt reduction of TMI absolute cavity responsivity was observed, after investigation, it was found that, a spider and its web inside the cavity which was then removed from the precision aperture. This optical obstruction was determined to be the reason of the measurement differences (Stoffel and Reda, 2008).

3.1.1.2 Shortwave and Longwave Outdoor Radiometer Calibration

NREL's unique BORCAL process is ISO/IEC 17025 accredited and, as DOE's lead laboratory for solar radiation, provides WRR-traceable radiometer calibrations. While conducting active research to develop standards that reduce calibration uncertainty, this capability also ensures accurate measurements for various research projects supported by SETO. Calibration services using the BORCAL process are offered for a fee to external customers, and are free for internal customers.

During the FY 2019–2021, BORCAL was carried out in compliance with ISO 17025 accreditation for a total of 486 shortwave and 64 longwave radiometers (Table 1). Figure 3 shows an example of a BORCAL event. These radiometers came from NREL, various labs, and industry. Further, during this period, the NREL-SRRL team performed all necessary upgrades to the Radiometer Calibration and Characterization software to improve the process of calibration.

Table 1. Total Number of Radiometers Calibrated during FY 2019–FY 2021

Fiscal Year	Shortwave Radiometers	Longwave Radiometers
19	190	24
20	116	14
21	180	26

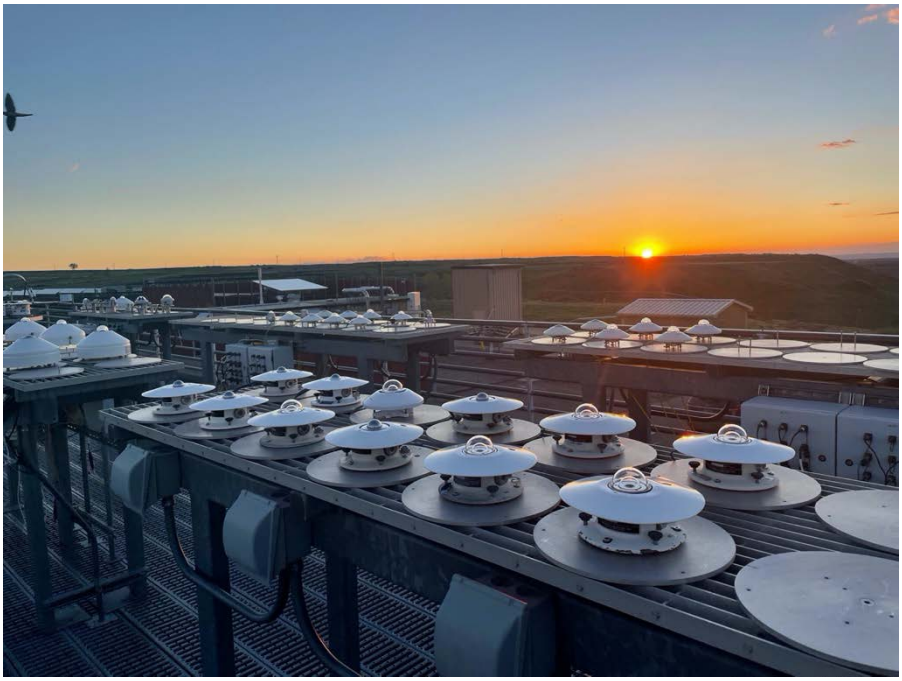

Figure 3. BORCAL shortwave and longwave setup

Moreover, the NREL-SRRL team continues to develop a process for the manufacture and sell of the absolute cavity pyrgeometer (ACP) at NREL to interested customers. Thus far, the ACP has been sold to the German Meteorological Office, Australian Bureau of Meteorology, and Japanese Meteorological Agency.

The NREL-SRRL team also continues to provide timely outreach of the ACP's relevance through publications and conference presentation. Recently, Reda et al. (2020), presented a paper at the IPC-XIII on their work, titled "Using an Absolute Cavity Pyrgeometer to Validate the Calibration of a Transfer Standard Pyrgeometer Outdoors, Independent from the Reference Value of the Atmospheric Longwave Irradiance." The presentation detailed the unique method that was developed to calibrate pyrgeometers to improve the measurement uncertainty. The ACPs and pyrgeometer passive infrared model were deployed outdoors (Figure 4). The passive infrared was placed on a temperature controller like the ACP's temperature controller.

Figure 4. Outdoor setup of the (left to right) ACP95F3, ACP10F3, and passive infrared on top of temperature controllers

The responsivity of the pyrgeometer is then calculated by cooling its case temperature, as described in Eq. 1.

$$W_{atm} = K_1 V + K_2 W_r + K_3 (W_d - W_r) \qquad \text{Eq. 1}$$

Where:

- W_{atm} is the atmospheric longwave radiation in W/m^2.
- K_2 and K_3 are the calibration coefficients of the pyrgeometer, calibrated at the Physikalisch-Meteorologisches Observatorium Davos or using a blackbody (Note: A blackbody calibration source is an instrument for calibration of an infrared temperature sensor, a pyrgeometer.)
- K_1 is the reciprocal of the pyrgeometer's responsivity, calculated from the outdoor calibration described Eq. 5.
- V is the pyrgeometer thermopile output, in microvolts.
- W_r is the pyrgeometer receiver radiation, equal to $\sigma \times T_r^4$ where:
    - $T_r = T_c + K_4 \times V$
    - σ is the Stefan-Boltzmann constant, 5.6704×10^{-8} W/m^2K^4
    - T_C is the pyrgeometer case temperature in Kelvin.
    - K^4 is the thermopile efficiency factor, 1/(S × n × E)=0.0007044 K uV^{-1}, where:
        - S is the Seebeck coefficient, equal to 39 V/K.
        - n is the number of thermopile junctions, equal to 56 junctions.
        - E is the thermopile efficiency factor, equal to 0.65 (manufacturer specification).

- W_d is the pyrgeometer dome radiation, equal to $\sigma \times T_d^4$, where T_d is the dome temperature in Kelvin.

Eq. 1 is rewritten in the following form:

$$W_{out} = W_{atm} - W_{net} = W_{atm} - K_1 V \qquad \text{Eq. 2}$$

Where:

- W_{net} is the net irradiance measured by the pyrgeometer thermopile.
- W_{out} is the outgoing irradiance from the pyrgeometer.

$$W_{out} = K_2 W_r + K_3 (W_d - W_r) \qquad \text{Eq. 3}$$

A fundamental principle for this calibration procedure is to reduce the outgoing irradiance while the atmospheric longwave irradiance (W_{atm}) is constant, i.e., stable during clear-sky conditions to within 1 W/m^2 from the start to the end of the calibration, at least 7 minutes. Reducing W_{out} was achieved by cooling the pyrgeometer's case using the temperature controller. While reducing W_{out}, all signals from the pyrgeometer (i.e., thermopile output voltage, T_d, and T_r) were measured every 10 seconds (i.e., thermopile output voltage, T_d, and T_r). Differentiating Eq. 2 with respect to time then yields:

$$\frac{dW_{out}}{dt} = \frac{dW_{atm}}{dt} - K_1 \frac{dV}{dt} \qquad \text{Eq. 4}$$

If W_{atm} is assumed constant, Eq. 4 then yields:

$$K_1 = \frac{-dW_{out}}{dV} \qquad \text{Eq. 5}$$

Eq. 5 implies that the change in W_{out} versus the change in V yields K_1, which is independent from the absolute value of W_{atm}.

Once K_1 was calculated, using the previous procedure, Eq. 1 was used to calculate the measured atmospheric longwave irradiance for 2 hours. This procedure was repeated when the solar zenith angle was >95°.

Figure 5 shows the results of three test pyrgeometers using the transfer standard pyrgeometer, where K_2 and K_3 in Eq. 1 are calculated using the broadband calibration. K_1 is calculated by deploying the test pyrgeometers with the Transfer Standard Pyrgeometer outdoor during nighttime clear-sky conditions for 2 hours to account for the spectral response of the pyrgeometers and the spectral mismatch between the broadband and the atmospheric longwave irradiance. The test pyrgeometers are then used as a secondary transfer reference to calibrate other pyrgeometers during nighttime under all sky conditions.

The irradiance measured by the pyrgeometer (PIR) was compared against the irradiance measured by ACP95F3. The overall uncertainty (U_{95}) with a confidence level of 95% (k=~2) was calculated by means of the square root of the sum of the squares method by using U_{95ACP} equals ±2 W/m^2 with respect to SI and U_{95PIR} equals ±2.88 W/m^2 with respect to ACP; therefore, U_{95} equals ±3.51 W/m^2 with respect to SI.

These results suggest that this pyrgeometer calibration method might be useful in addressing the international need for a transfer standard pyrgeometer traceable to the International System of Units. Note: The current calibration and traceability of pyrgeometers is based on the World Interim Standard Group.

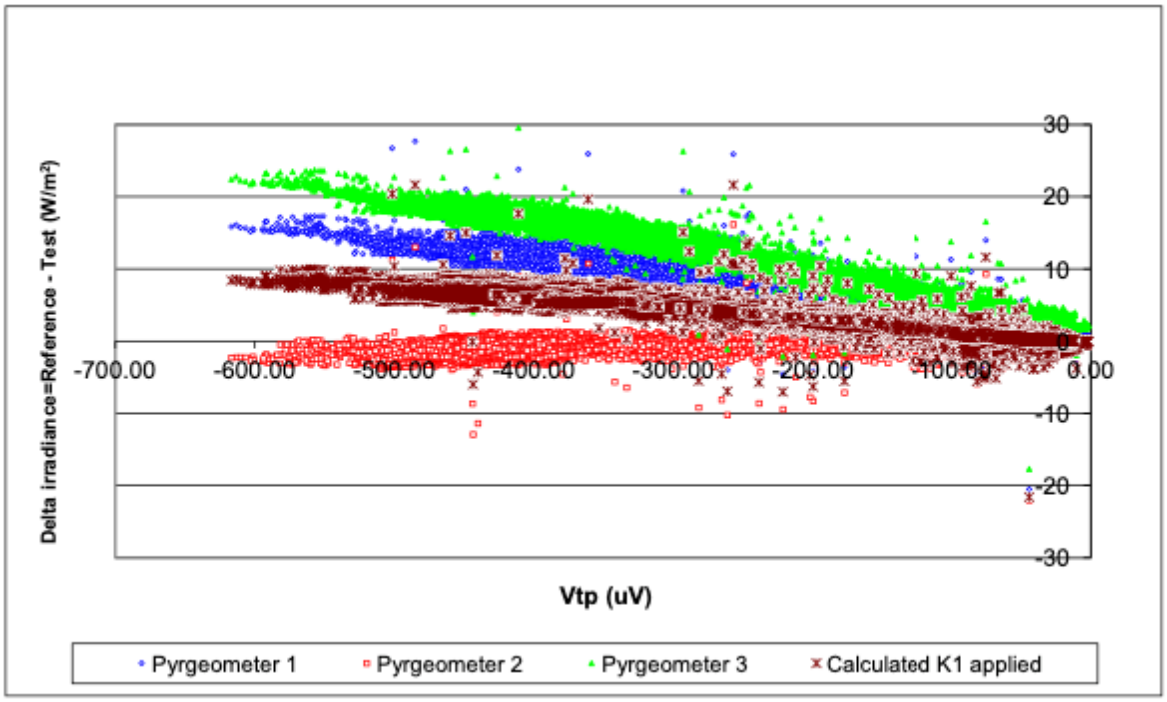

Figure 5. Calibrating three test pyrgeometers using the transfer standard pyrgeometer

3.1.1.3 Optical Metrology Laboratory for Spectral Irradiance Calibration

The NREL team continues to advance spectral solar irradiance measurement and calibration capabilities. A group of standard lamps from the National Institute of Standards and Technology (NIST) serves as the DOE/NREL spectral measurement reference. These lamps are used to calibrate spectroradiometers.

Spectroradiometers are used for many solar energy applications to understand the spectral properties of the PV modules. These spectroradiometers are most frequently used for measuring the spectrum of solar simulators or outdoor natural sunlight. These are critical measurements for many solar energy stakeholders, including NREL, because it is important to know the performance of PV modules and cells under a known set of standard spectral reporting conditions, for example.

Spectral irradiance is typically measured with a spectroradiometer; the spectroradiometer must be calibrated with traceability to national or international standards, such as those maintained by NIST (Yoon and Gibson 2010). The NREL Optical Metrology Laboratory maintains NIST traceable lamp standards of spectral irradiance. These lamps are used to calibrate spectroradiometers that indicate the irradiance ($W/m^2/nm$) as a function of wavelength (nm). The laboratory is responsible for spectral field measurements, instrumentation troubleshooting/repair, and consultation. During FY 2019 and FY 2021, the NREL Optical Metrology Laboratory

completed an A2LA external audit for the ISO/IEC 17025 accreditation for spectral irradiance calibration at NREL—and passed with no deficiencies, certifying that NREL provides reliable testing, measurement, and calibration services. ISO/IEC 17025 is an internationally recognized technical quality management system standard for laboratory accreditation. NREL was assessed against the general criteria found in ISO/IEC 17025: General Requirements for the Competence of Testing and Calibration Laboratories.

Similarly, the NREL-SRRL team continued to calibrate and characterize spectroradiometers and solar simulators (Table 2). For example, the NREL-SRRL installed and calibrated the Spectrafy SolarSIM-G global horizontal spectral modeling device. The calibration was done in outdoor conditions at the NREL-SRRL and MIDC was updated to support this new device. Prior to the global horizontal deployment, the device was calibrated against the EKO Instruments' WISER system on the two-axis tracker (Figure 6).

Table 2. Total Number of Spectral Devices Calibrated during FY 2019–FY 2021

Fiscal Year	Spectroradiometers	Solar Simulators	Filtered Radiometers	Reflection/ Transmission
2019	13	15	1	3
2020	14	7	19	0
2021	17	10	0	2

Figure 6. SolarSIM-G (mounted highest on the left side of the tracker) being calibrated against the EKO WISER on a global normal (two-axis) tracker

3.1.1.4 Solar Resource Gap-Filling and Forecasting

NREL, in collaboration with the Department of Applied Mathematics and Statistics at the Colorado School of Mines (Mines), applied a machine learning-based forecasting method using

measured and modeled historical data sets while investigating the presence of long-term trends in those data sets. This research will directly benefit the field of solar measurements and modeling by providing additional useful information to PV plant operators, solar developers, and financiers. Methods and results from this research will possibly have applicability in many other disciplines, including geography, ecology, environmental science, aerospace engineering, and forestry, among others.

The first project focused on a data imputation process to obtain a complete and reliable temporal and spatial data series. This study focused on imputing temporal scales by applying random and artificial data gaps and then implementing eight imputation methods, including the Kalman filtering and smoothing and stine interpolations. These methods were implemented on 1-minute to half-hourly irradiance data for 1 year using a few locations from the NSRDB and a ground measurement data set. The ground measurement data were obtained from seven National Oceanic and Atmospheric Administration Surface Radiation Budget Network (SURFRAD) stations and modeled data from the NSRDB Version 3.

The following eight imputation methods were selected:

1. **Kalman filtering and smoothing for structural time series**: Kalman filtering, also known as linear quadratic estimation, produces estimates of unknown variables from a series of measurements observed over time by estimating a joint probability distribution over the variables for each time frame. Structural time-series models are set up in terms of their components, which have a direct interpretation (Grewal 2011; Harvey 1990; Welch and Bishop 1995).
2. **Kalman filtering and smoothing for the state-space representation of an ARIMA model:** Kalman filtering is applied to an autoregressive integrated moving average (ARIMA) model, which uses several lagged observations of time series to forecast observations (Grewal 2011; Harvey 1990; Welch and Bishop 1995).
3. **Linear interpolation:** Linear interpolation is a curve-fitting method that uses linear polynomials to construct data points within the discrete range of known data points.
4. **Spline interpolation:** Spline interpolation is a curve-fitting method that uses a piecewise polynomial interpolant to construct data points within a discrete range of known data points (Lyche and Schumaker 1973).
5. **Stine interpolation:** Stine interpolation is a curve-fitting method that uses piecewise rational interpolation to replace missing values (Stineman 1980).
6. **Simple moving average:** Simple moving average calculates an average of the last **n** observations (Johnston et al. 1999; Ekhosuehi and Dickson 2016).
7. **Linear weighted moving average:** Linear weighted moving average calculates an average of the last **n** observations through applying weighting factors that decrease in a linear fashion (Ekhosuehi and Dickson 2016).
8. **Exponential weighted moving average:** Exponential weighted moving average calculates of the last **n** observations through applying weighting factors that decrease exponentially, never reaching zero (Johnston et al. 1999; Ekhosuehi and Dickson 2016).

Figure 7 shows the flowchart of the process of the gap-filling method implementation. The performance of the models was checked. To further measure the method performance, the strings of consecutive NA values in the NRSDB Kt series, both originally missing and synthetically created gaps, were partitioned into varying bin sizes. Each method's imputation performance was

measured for all six NA bin sizes across three separate groups: (1) Bin 1: 1 consecutive NAs, (2) Bin 2: >1 consecutive NA, (3) Bin 3: 1–2 consecutive NAs, (4) Bin 4: >2 consecutive NAs, (5) Bin 5: 1–3 consecutive NAs, and (6) Bin 6: >3 consecutive NAs. Dividing the bin sizes into three separate groupings allowed for testing the sensitivity of the imputation methods to gap size. For example, the following figures show that the spline interpolation's imputation performance significantly suffered when implemented on large gap sizes.

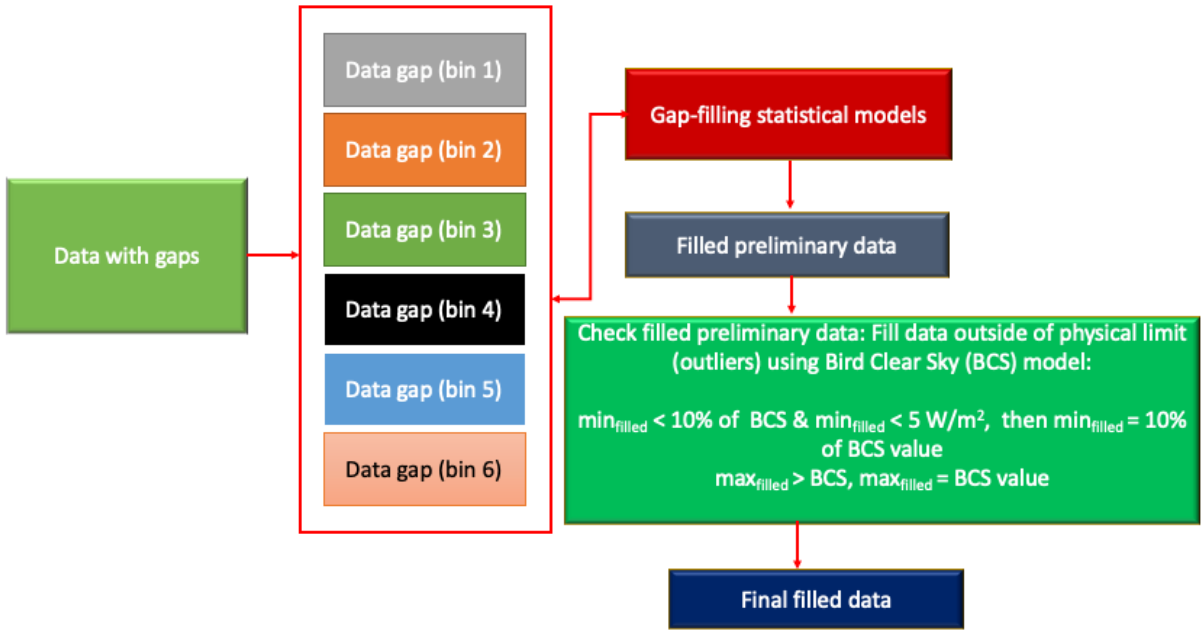

Figure 7. Flowchart of the data imputation process for the solar irradiance data

The results demonstrated that some of the simpler methods, such as the stine and linear interpolation methods, were the relatively best models based on the statistical metrics for imputing NSRDB and ground measurement data, respectively.

Figure 8 shows the mean bias error (MBE) and root mean square error (RMSE) results for each method and bin size for the Bondville, Illinois, NSRDB site. Spline interpolation performed significantly worse than the other methods in imputing the missing values for bins 2, 4, and 6. The remaining methods performed similarly for all bin sizes except Bin 2, in which the stine interpolation had a comparatively low RMSE value. For graphical purposes, the absolute values of the MBE were used to visually compare the bias across the methods. Like with RMSE, the spline interpolation had the highest bias across bins 2, 4, and 6. The method also had noticeably higher bias than the others for Bin 1. The stine interpolation and the moving average methods exhibited the lowest bias; however, the Kalman filtering methods and linear interpolation did not have comparatively significant higher bias.

For the ground measurement, linear interpolation had the smaller resulting RMSE, though these values did not significantly differ for the stine interpolation. The methods performed most similarly for the Desert Rock, Nevada, location, which has more clear-sky days and therefore fewer missing observations than the other locations.

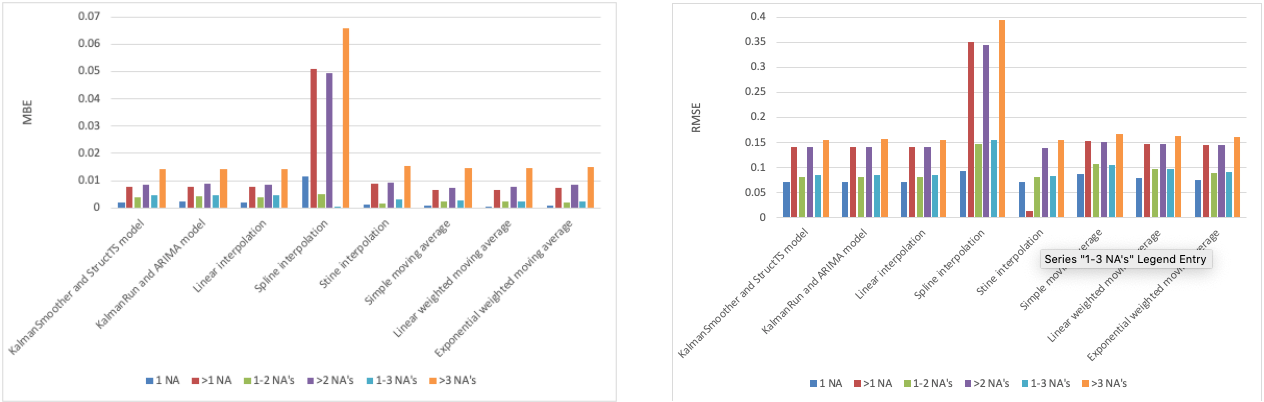

Figure 8. Resulting MBE and RMSE values by imputation method across six NA bin sizes for the Bondville, Illinois, NSRDB data

However, testing the algorithm in 15 ground measurement stations located in India demonstrated a selection of different imputation models; therefore, NREL and Mines made the code versatile to select one model for any location based on the statistical metrics. A suitable data imputation method would assist researchers in obtaining continuous observation of solar radiation.

The second project that NREL and Mines performed was the evaluation of deep learning methods for short- and long-term solar irradiance prediction. This study considered various machine learning prediction models, such as a long short-term memory (LSTM) network, ARIMA, a recurrent neural network, and gated recurrent units to predict daily, weekly, and monthly solar irradiance using the data set from the NSRDB. The study evaluated the skills of these models in predicting the various time horizons of solar irradiance for a few locations around the contiguous United States that represent various climatic conditions. Results from the prediction and evaluation demonstrated that the prediction skills vary temporally and spatially. The results demonstrated that the ARIMA model performed best in terms of MBE, RMSE, and mean absolute error (MAE) compared to deep recurrent neural network methods for both short-term and long-term solar irradiance prediction.

The NSRDB data consist of 22 years of global horizontal irradiance (GHI) observations in 30-minute intervals. The time series are complete with no data gaps. First, for each location, a log-transform was applied to stabilize the variance in the observations. The transform normalized the distribution of the series as well as possible. Next, three subseries of the data were created as follows: the daily totals of GHI, the monthly mean of the daily GHI totals, and the weekly mean of the daily GHI totals. For each subseries, seasonality was removed. For the monthly mean of the daily GHI totals, the seasonality was removed by subtracting the mean for a given month of the year from all data for that month. Similarly, the seasonality was removed from the weekly mean of the daily GHI totals by subtracting the mean for a given week of the year from all data for that week. The seasonality was removed from the daily GHI totals by subtracting the mean for a given day of the year from all data for that day. Last, each time series was converted into a supervised learning problem—as is required for neural network training in Python—such that the dependent variable is a lagged (t-1) version of the response, or the series at time t.

Figure 9 shows an example of the results of short-term predictions for the monthly mean of the daily GHI totals for the NREL location. Each method performed similarly in capturing the

cyclical behavior of the test values. There is no discernible graphical difference among the methods' predictions; however, when analyzing the statistical metrics, the LSTM resulted in the lowest values for RMSE and mean absolute percentage error (MAPE). ARIMA had the lowest bias highlighted in the MBE result. Overall, the metrics for all four methods were not significantly different. The average run time for the ARIMA model was less than 1 minute, whereas the average run times for the recurrent neural network, LSTM, and gated recurrent units were 4 minutes, 8 minutes, and 7 minutes, respectively.

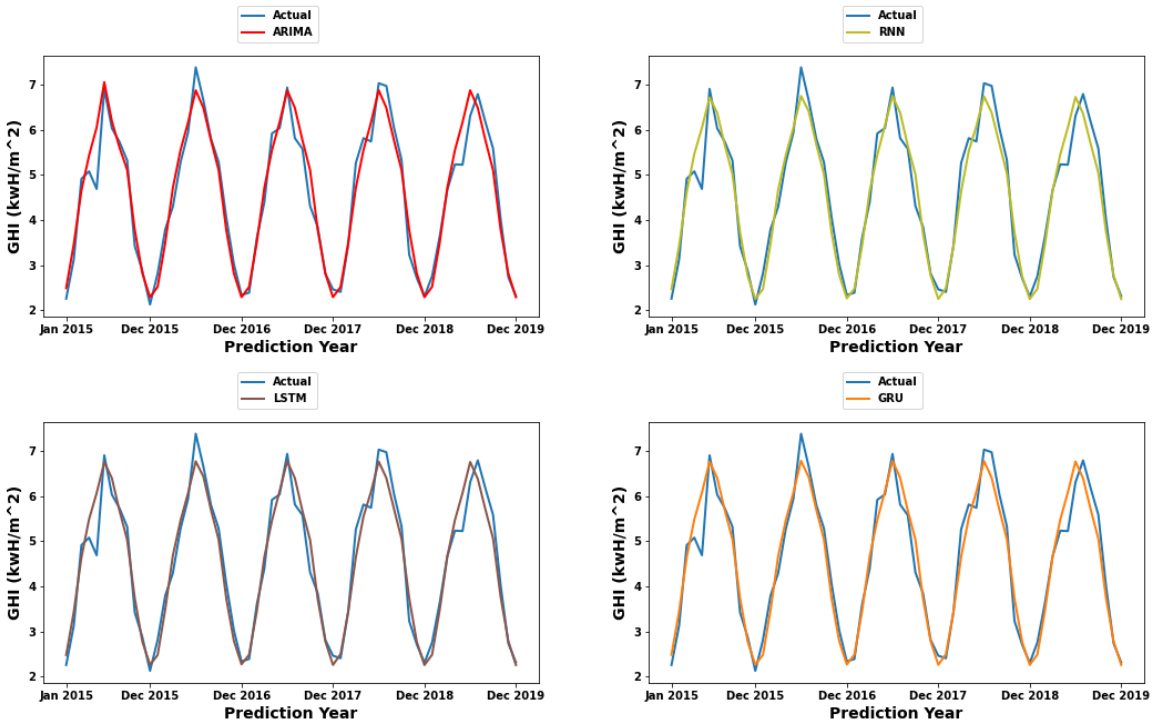

Figure 9. One-step-ahead prediction for the monthly mean of the daily GHI totals (NREL location)

3.1.1.5 Cooperative Research and Development Agreements

The NREL-SRRL, in collaboration with industry partners, develop and carry out CRADAs with the intent to evaluate radiometers and spectroradiometers. This also provides a framework for industry partners to conduct research to improve and develop new radiometric devices and applications in the future. The overall objective is to provide more accurate, site-specific, and reliable solar resources information required by industry to increase the deployment and improve the operations of PV and concentrating solar power plants.

During FY 2019–FY 2021, NREL carried out multiple collaborations—such as those with EKO Instruments, Kipp & Zonen, and Arable Labs—to test new instruments and evaluate radiometers deployed at the NREL-SRRL. The following is a summary of the analysis and results that were accomplished in collaboration with EKO Instruments. Some of the instruments deployed under this CRADA at NREL-SRRL are illustrated in Figure 10.

Figure 10. (Top left) “Fast response" and "spectrally flat" EKO MS-80 pyranometer, (top right) MS-80 on a rotating shadow band for measuring GHI and DHI, and (bottom) EKO MS-57 with low thermal offset behavior and fast thermopile response

NREL and EKO Instruments collaborated to analyze the performance of radiometers and spectroradiometers.

One-minute data from eight spectrally flat Class A pyranometers measuring GHI for a period of 1 year (June 1, 2020, to July 2, 2021, Comparison Provision 3) were collected from the MIDC (Comparison Provision 8). Table 3 shows the list of pyranometers from various manufacturers, including EKO models. Two of the EKO models (MS-80 and MS-80S) employ new thermopile technology with a faster temporal response (<0.5 second) than traditional thermopile ISO 9060:2018 Class A pyranometers (<5 second).

Table 3. Pyranometer List (Comparison Provisions 1 and 2)

Model	QTY	Correction	Ancillary Equipment	Calibrated by	Manufacturer	ISO 9060:2018 Classification
CMP22 (labeled as CMP22-vencorr)	1	Thermal offset	External ventilator	BORCAL (NREL)	Kipp & Zonen	Spectrally flat Class A

Model	QTY	Correction	Ancillary Equipment	Calibrated by	Manufacturer	ISO 9060:2018 Classification
CMP22 (labeled as CMP22-1)	1	Thermal offset	---	BORCAL (NREL)	Kipp & Zonen	Spectrally flat Class A
CMP11	1	Thermal offset	---	BORCAL (NREL)	Kipp & Zonen	Spectrally flat Class A
SR25	1	---[a]	---	BORCAL (NREL)	Hukseflux	Spectrally flat Class A
MS-80	1	---	---	BORCAL (NREL)	EKO Instruments, Inc.	Fast response Spectrally flat Class A
MS-80S	1	---	---	Normal incidence (EKO)	EKO Instruments, Inc.	Fast response Spectrally flat Class A
MS-802	1	Thermal offset	---	BORCAL (NREL)	EKO Instruments, Inc.	Spectrally flat Class A
SPP	1	Thermal offset	External ventilator	BORCAL (NREL)	Eppley Laboratory, Inc.	Spectrally flat Class A

[a] The manufacturer-specified "temperature" correction was applied.

As shown in Table 3, some pyranometers contain a thermal offset correction supplied by NREL's BORCAL process. Many studies—including Sengupta et al. (2021), Michalsky et al. (2017), Habte et al. (2017), Younkin and Long (2003), and Dutton et al. (2001)—affirm that a thermal offset correction provides better-quality radiometric data in some radiometers. A reference data set with the lowest possible uncertainty was obtained using a component sum method using a Kipp & Zonen model CHP1 pyrheliometer and a Kipp & Zonen CM22 diffuse horizontal irradiance (DHI) shaded pyranometer (Habte et al. 2017; Habte et al. 2016; Wilcox and Myers 2008).

The MS-80S was calibrated at EKO, but the seven pyranometers were calibrated at NREL using the BORCAL process; therefore, data normalization was necessary to remove calibration biases. The normalization was carried out using Eq. 6 and Eq. 7 by isolating the irradiance data under all sky conditions between 44° and 46° solar zenith angles and summing and then obtaining the ratio of all the data in this solar zenith angle range for the reference data and a unit-under-test pyranometer for the study period (June 1, 2020, to July 2, 2021). The solar zenith angle range conforms to the NREL convention of reporting all broadband radiometer calibrations at a 45° solar zenith angle (Habte et al. 2017; Habte et al. 2016). The ratio for each test radiometer was then used to acquire the new normalized irradiance value by multiplying each test irradiance value for the time interval by the normalization ratio (Eq. 6):

$$Normalization\ Factor = \frac{\sum I_{Ref_{44^\circ\ to\ 46^\circ}}}{\sum I_{UUT_{44^\circ\ to\ 46^\circ}}} \qquad \text{Eq. 6}$$

Where $I_{UUT\ 44^\circ\ to\ 46^\circ}$ is the irradiance data under all sky conditions for the unit under test within the 2° solar zenith angle bin and $I_{Ref\ 44^\circ\ to\ 46^\circ}$ is the irradiance data of the reference instrument within the same solar zenith angle range.

The new normalized irradiance data from the unit under test were then computed as (Eq.7):

$$I_{UUT(New)} = I_{UUT} * Normalization\ Factor \qquad \text{Eq. 7}$$

Missing data, which accounted for approximately 25% of the 1-year data, were removed from the analysis. This data gap was for EKO model MS-80S; however, this data gap was resulted from an issue in the data acquisition system. The period of the missing data set was removed from all seven remaining pyranometer data sets before the analysis to ensure a rigorous comparison of the pyranometer data. Moreover, the analysis included data only for solar zenith angles less than 80°, which excludes nighttime, early morning, and late afternoon data.

After implementing data normalization and filtering, NREL's SERI-QC software package, a data quality assessment tool, was employed for the data set from all eight pyranometers. As stated in the SERI-QC software user's manual (Maxwell, Wilcox, and Rymes 1993), the software uses three component data—GHI, direct normal irradiance (DNI), and DHI—and calculates the clearness index (K) derived by standardizing the GHI, DNI, and DHI irradiance data to extraterrestrial solar radiation at the top of the atmosphere. These standardized quantities are represented by Kt, Kn, and Kd, respectively. The K values of any one of the three components can be computed from the other two. Further the K values are shown in Figure 11 in conjunction with data quality flags. As described in Maxwell, Wilcox, and Rymes (1993), the data quality flags range from 0–99; the latter refers to missing data, which was taken care of during the data filtering process. NREL applied additional filtering or exclusion processes by using the remaining data quality flags. Data quality flags from 10–97 signify failed two- or three-component tests (flags 10–93); and data fall into a physically impossible region where Kn > Kt by K-space distances of 0.05–0.10 (flag 94), 0.10–0.15 (flag 95), 0.15–0.20 (flag 96), or ±0.20 (flag 97). These criteria of excluding data with data quality flags of 10–97 were implemented when these flags occurred in four or more of the eight pyranometers. This exclusion accounted for approximately 1.5% of the data set, which is in addition to the 25% missing data mentioned previously.

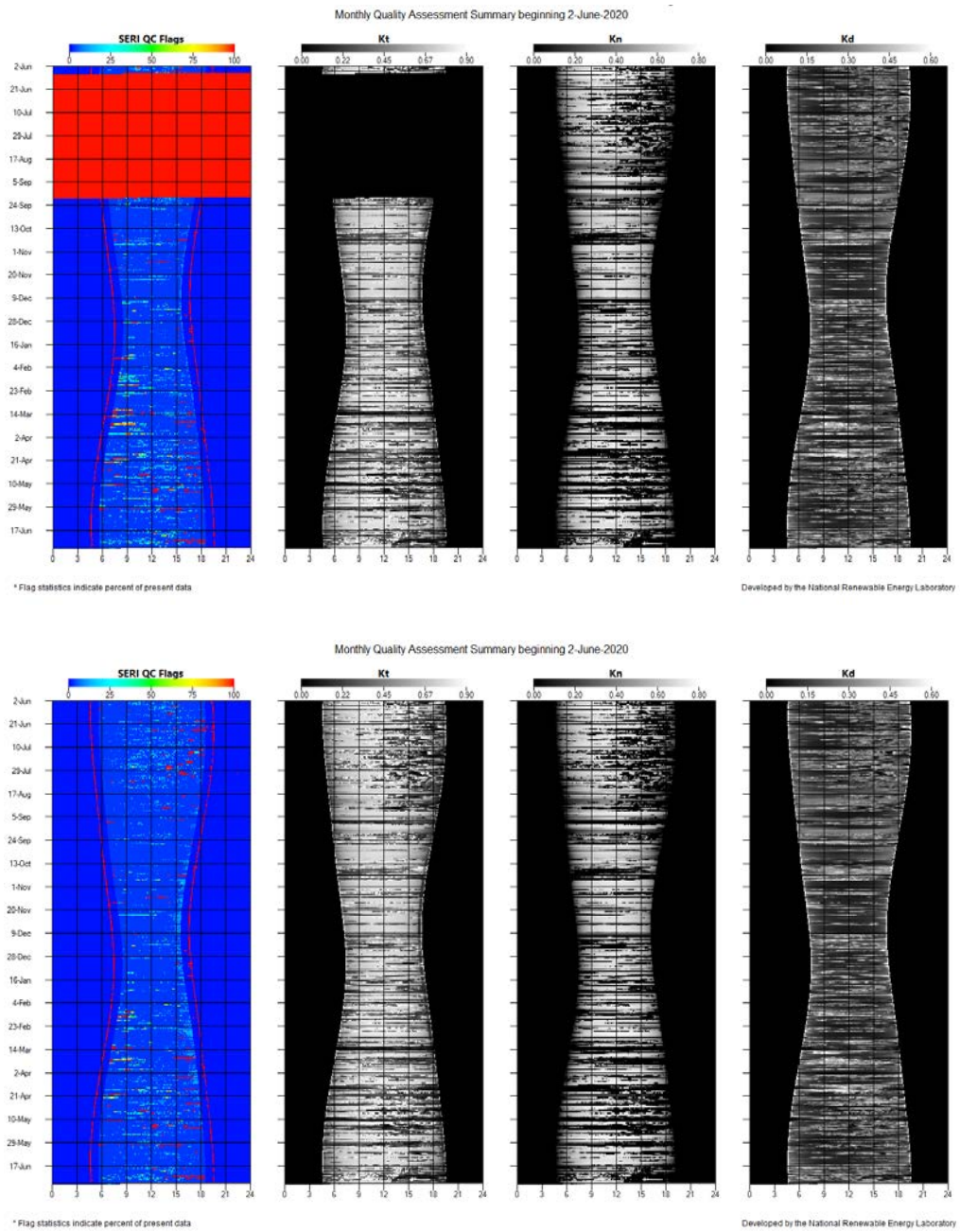

Figure 11. Example of SERI-QC software data quality assessment for the (top) EKO model MS-80S and (bottom) Kipp & Zonen model CMP22_vencor. The clearness index, Kt, describes these two pyranometers. The reference Kn and Kd are from the BMS DNI and DHI, respectively. Note: The MS-80S was missing 3 months of data in 2020 resulted from a data acquisition problem.

The leftmost chart in Figure 11 shows the most severe flags from among the three components (Kt, Kn, and Kd) at each time interval. The lowest error levels are represented in dark blue, and the highest are shown in red.

The remaining three charts present the relative solar irradiance for the Kt, Kn, and Kd clearness ranges, where the dark represents overcast or missing data, and white represents clear-sky data.

To analyze the comparison among the different pyranometer models, a partitioning of the sky condition at each time stamp was implemented. A PVLIB clear-sky algorithm by Reno and Hansen (2016) was used to distinguish between clear and cloudy skies.

The analysis was done for each unit-under-test instrument relative to the reference instrument under various sky conditions. The results of the analysis are shown in Figure 12, and for ease of understanding, the results of the comparison were partitioned into 10° solar zenith angle bins. Each blue box represents a 10° bin, and it also represents the upper and lower quartiles (also called an interquartile range) of the data in each bin. The circle in each blue box is a mean, and the black line signifies the median value. Ninety-nine percent of the data set is within the whiskers; beyond the whiskers are outliers, which are plotted by dot symbols.

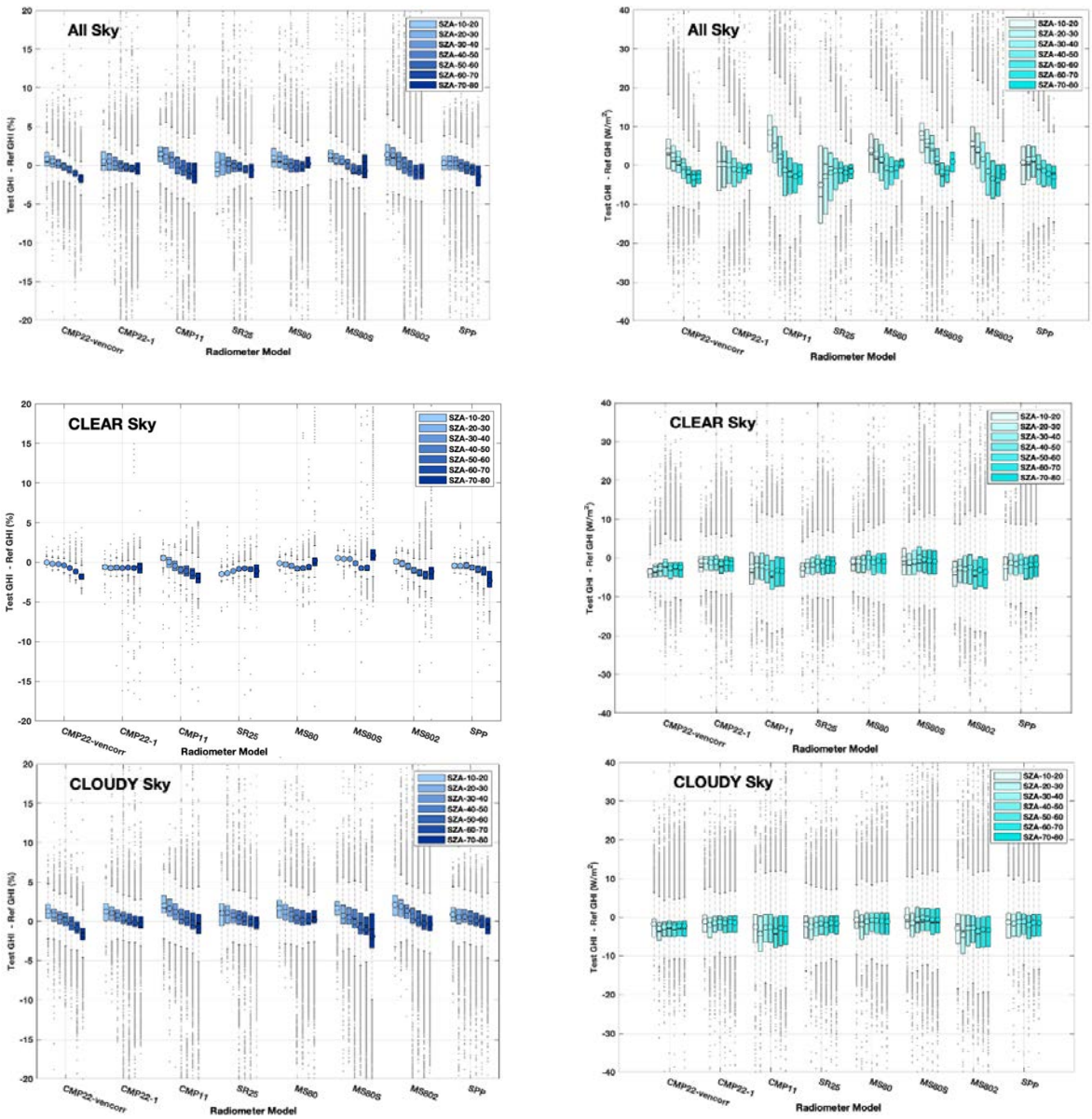

Figure 12. Comparison of the eight pyranometers relative to the reference data under various sky conditions. The left column is bias in percentage, and the right is in W/m^2.

The comparison demonstrated that Class A pyranometers on average have small bias relative to the reference data. Under clear-sky conditions, the interquartile range is within approximately ±1% and ±2 W/m^2. On the other hand, models MS-802 and CMP11 showed relatively higher deviation than the Class A pyranometers. Under cloudy-sky and all sky (cloudy + clear) conditions, the deviation is slightly higher than the clear-sky biases, and, as expected, there are fewer outliers under clear skies.

Further, the external ventilation system for the CMP22-vencorr and SPP appear to assist in improving the relative accuracy of the pyranometer data that are deployed outdoors and exposed to various environmental and meteorological conditions. Under clear skies, the ventilation system reduced the number of outliers. Outliers are mainly caused by snow, frost, soiling, bugs, etc.; therefore, as previously reported, the advantage of external ventilators is twofold—not only does the external ventilation system assist in reducing errors caused by snow, frost, etc., but it also assists in stabilizing the pyranometer body temperature, which, in turn, reduces thermal offset errors (Sengupta et al. 2021; Michalsky et al. 2017; Habte et al. 2016; Younkin and Long 2003; Dutton et al. 2001). The remaining pyranometers, including the EKO MS-80 and MS-80S, are not equipped with external ventilation systems; therefore, the data are prone to outliers when compared to a ventilated reference. However, these two pyranometers are fast-response radiometers (< 0.5 second) that can capture relatively fast-changing atmospheric conditions compared to the rest of the pyranometers, including the reference radiometers. Consequently, some of the outliers observed from these two radiometers (EKO MS-80 and MS-80S) can be accurate data, which might have happened under fast-changing atmospheric conditions, and they were not captured by the relatively slow time response of the reference instrument (5 seconds).

Similarly, a pyrheliometer (measuring DNI) comparison was completed. DNI data sets are traditionally collected using pyrheliometers mounted on a tracker. The NREL-SRRL BMS is equipped with multiple pyrheliometers mounted on trackers, including the EKO MS-57 pyrheliometer (Table 4). The evaluation of the pyrheliometers was done by comparing each unit under test to the reference DNI measurements, which were taken by a Kipp & Zonen CHP1 pyrheliometer. As described and reported previously, this reference pyrheliometer has lower calibration and measurement uncertainty; however, more studies are needed to corroborate these previous studies (Sengupta et al. 2021; Michalsky et al. 2017; Habte et al. 2016; Younkin and Long 2003; Dutton et al. 2001) because in recent years many technological advancements have been made in the radiometry industry to reduce uncertainty. It is safe to assume that any of the Class A pyrheliometers can be a reference pyrheliometer based on the results obtained in this study. Note also that the EKO MS-57 pyrheliometer—a fast-response, spectrally flat, Class A pyrheliometer—has an advantage in capturing and quantifying fast-changing atmospheric conditions compared to a similar class of spectrally flat pyrheliometers with relatively slower time responses.

The data filtering, normalization, and data quality assessment were carried out in the same way as the GHI analysis. Figure 13 shows the data quality assessment using SERI-QC.

Table 4. Pyrheliometer List

Model	QTY	Calibrated by	Manufacturer	ISO 9060:2018 Classification
CHP-1a	1	BORCAL (NREL)	Kipp & Zonen	Spectrally flat Class A
CHP-1	1	BORCAL (NREL)	Kipp & Zonen	Spectrally flat Class A
sNIP	1	BORCAL (NREL)	Eppley Laboratory, Inc.	Spectrally flat Class A
MS-57	1	BORCAL (NREL)	EKO Instruments, Inc.	Fast response Spectrally flat Class A

[a] Reference pyrheliometer

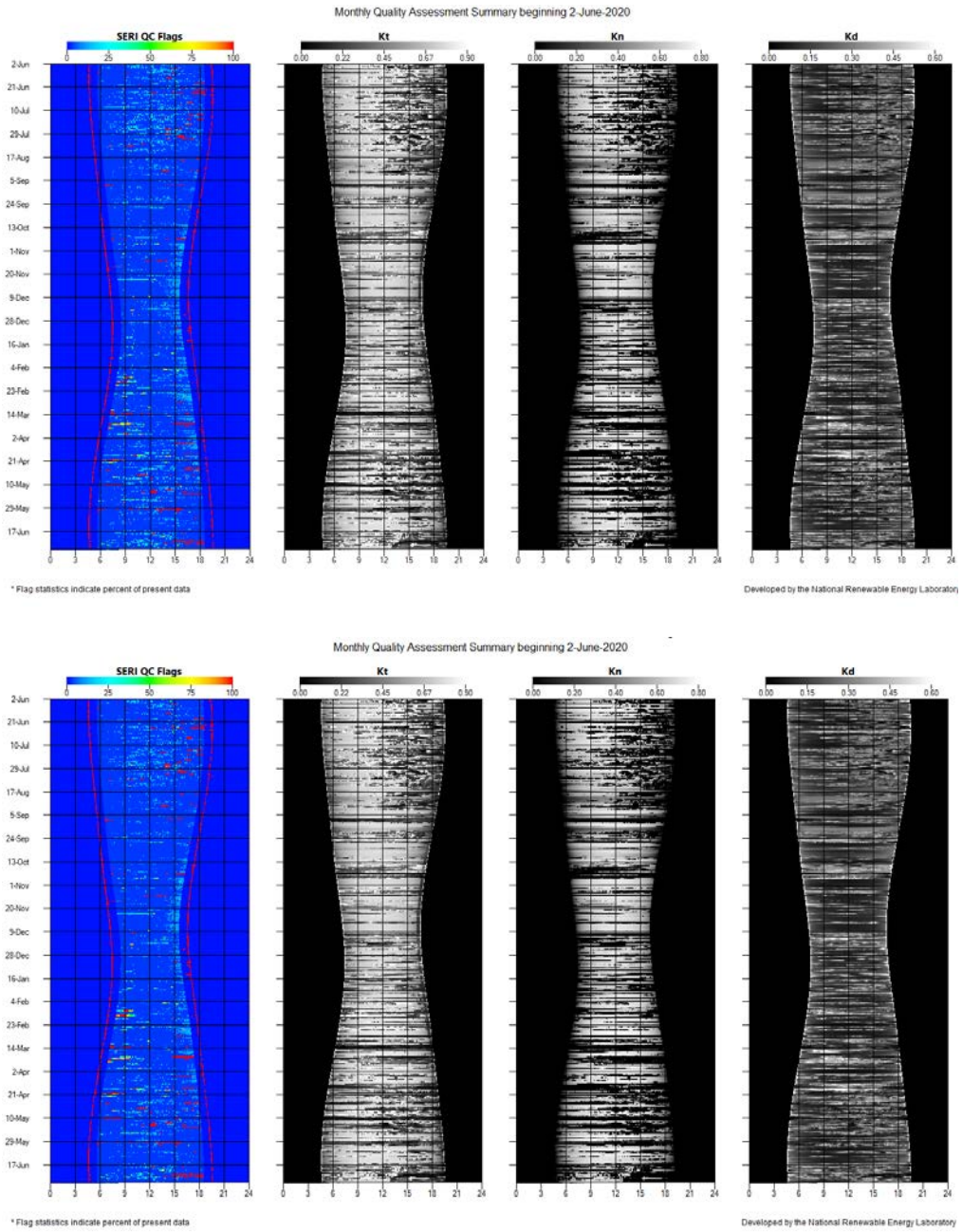

Figure 13. Example SERI-QC software data quality assessment for (top) an EKO MS-57 and (bottom) an Eppley Laboratory, Inc., sNIP. The clearness index, Kn, describes these two pyranometers. For SERI-QC, the units under test were compared with the NREL-SRRL BMS global and diffuse instruments.

Data sets from three pyrheliometers were included in this evaluation. Figure 14 demonstrates the comparison results under various sky conditions. The clear-sky conditions demonstrated smaller differences among the instruments than the cloudy sky conditions. For the GHI analysis, the differences were further divided into various solar zenith angle ranges; however, solar zenith angle dependence is not likely for pyrheliometers.

Under cloudy conditions, the EKO MS-57 demonstrated relatively higher differences. This could be because this particular pyrheliometer has a fast time response (<0.2 second), and therefore fast-moving clouds are captured in the measurement but not by the reference instrument, which has a response time <5 seconds.

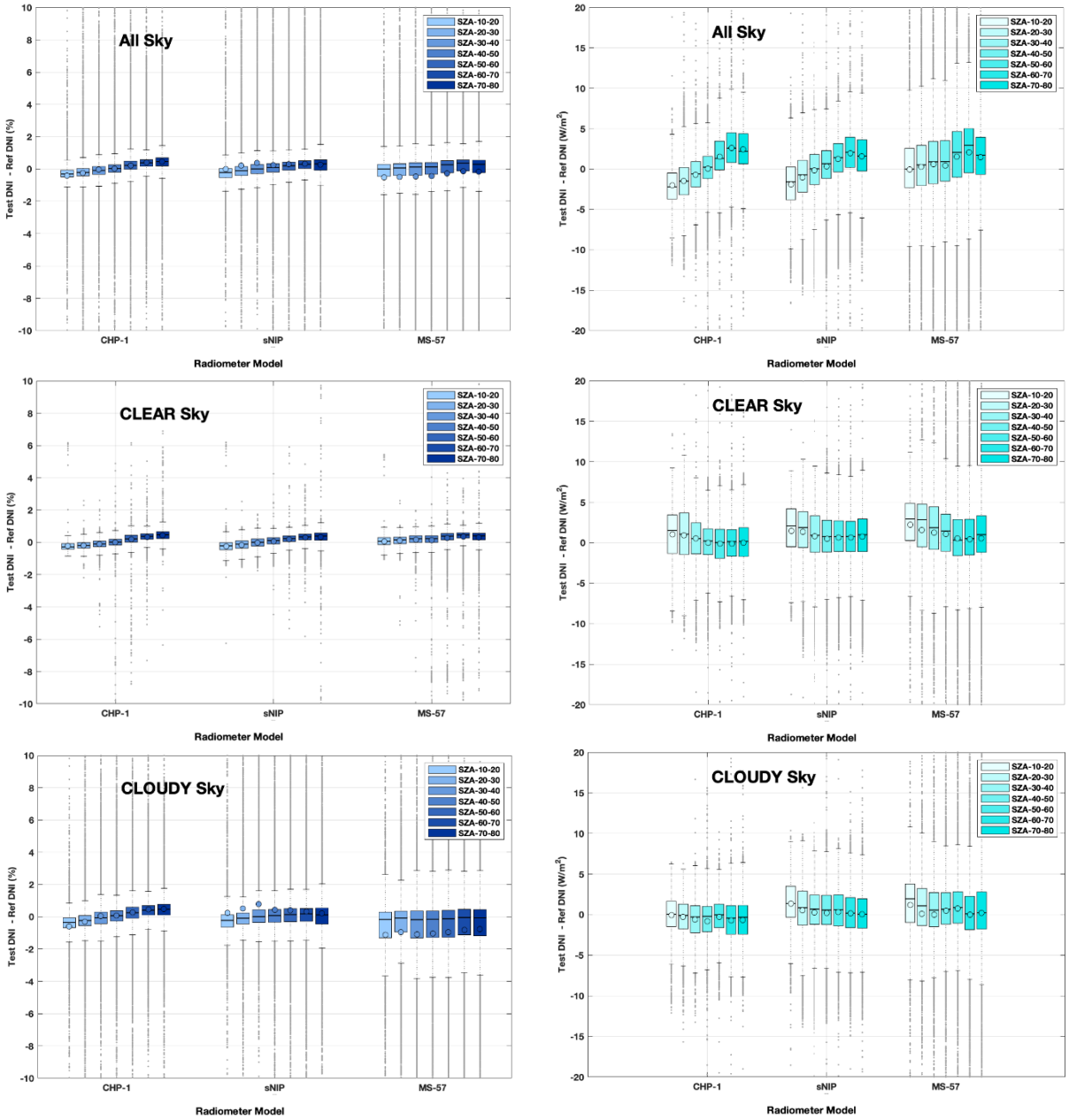

Figure 14. Comparison of the three pyrheliometers relative to the reference data under various sky conditions. The left column is bias in percentage, and the right is in W/m².

3.1.1.6 Operate and Update the Baseline Measurement System

The NREL-SRRL hosts a BMS that provides real-time, high-quality baseline data using instruments from various manufacturers for research and standards development. The BMS data sets are unique because of their completeness, are of the best achievable quality, and therefore

are used for measurement research and instrument development. All radiometers in the BMS are calibrated using either the BORCAL or NREL's optical metrology spectral calibration service. The BMS includes more than 100 instruments that measure independent components of solar radiation and meteorological conditions and represent current and past instruments from all major manufacturers. These data are widely used by researchers and industry, with more than 20,000 users per quarter, and they provide the basis for the development of standards. Collaborative research with universities and industry conducted using the BMS helps reduce the cost and improve the accuracy of radiometric measurements. NREL also conducts active research on identifying sources of uncertainty in measurements and developing processes to reduce those uncertainties.

3.1.1.7 Data Quality

Evaluating the performance of PV cells, modules, and arrays that form large solar deployments relies on accurate measurements of the available solar resource; therefore, determining the accuracy of these solar radiation measurements provides a better understanding of investment risks. This becomes especially important as deployment size and investment costs increase to the hundreds of millions of dollars. The accuracy of measurements is also important for acceptance testing and operations. NREL maintains a suite of the highest quality solar radiation measurement systems following the best practices for industry (Sengupta et al. 2021). These instruments provide a continuous stream of quality data for baseline research through the continuous application of data quality evaluations using NREL's SERI-QC software (Maxwell et al. 1993). The results of the assessment for FY 2016–FY 2021 are illustrated in Figure 15.

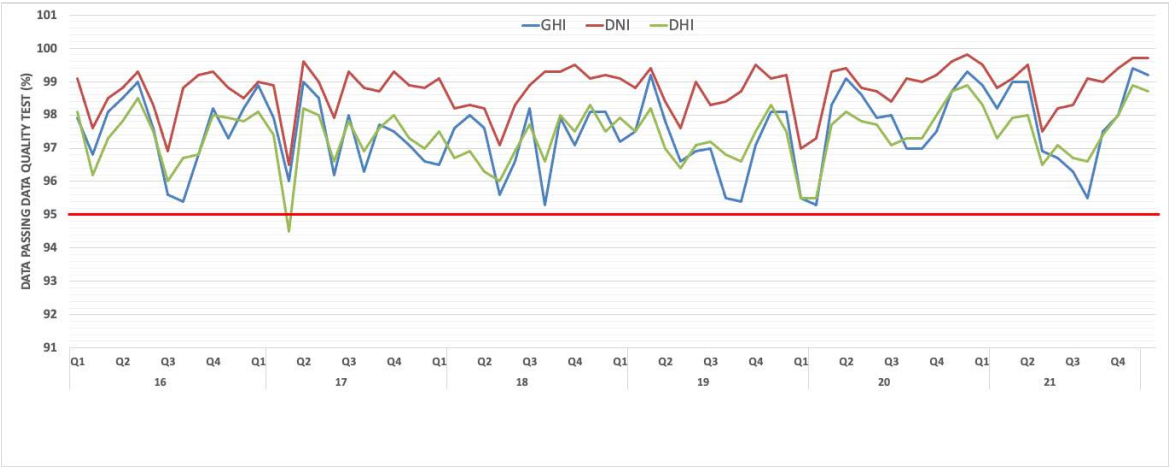

Figure 15. Quarterly MIDC data quality report

3.1.2 Dissemination of Data and Models

Through this activity, NREL collected and disseminated access to quality-controlled, traceable measurements to users in real time for the NREL-SRRL and other partner sites around the country that take quality solar radiation measurements throughout the United States. All historical and real-time measurement data are made available through the MIDC portal[4] (Stoffel

[4] See http://www.nrel.gov/midc/.

and Andreas 1981). Figure 16 shows the location distribution of the stations whose data are disseminated by the MIDC.

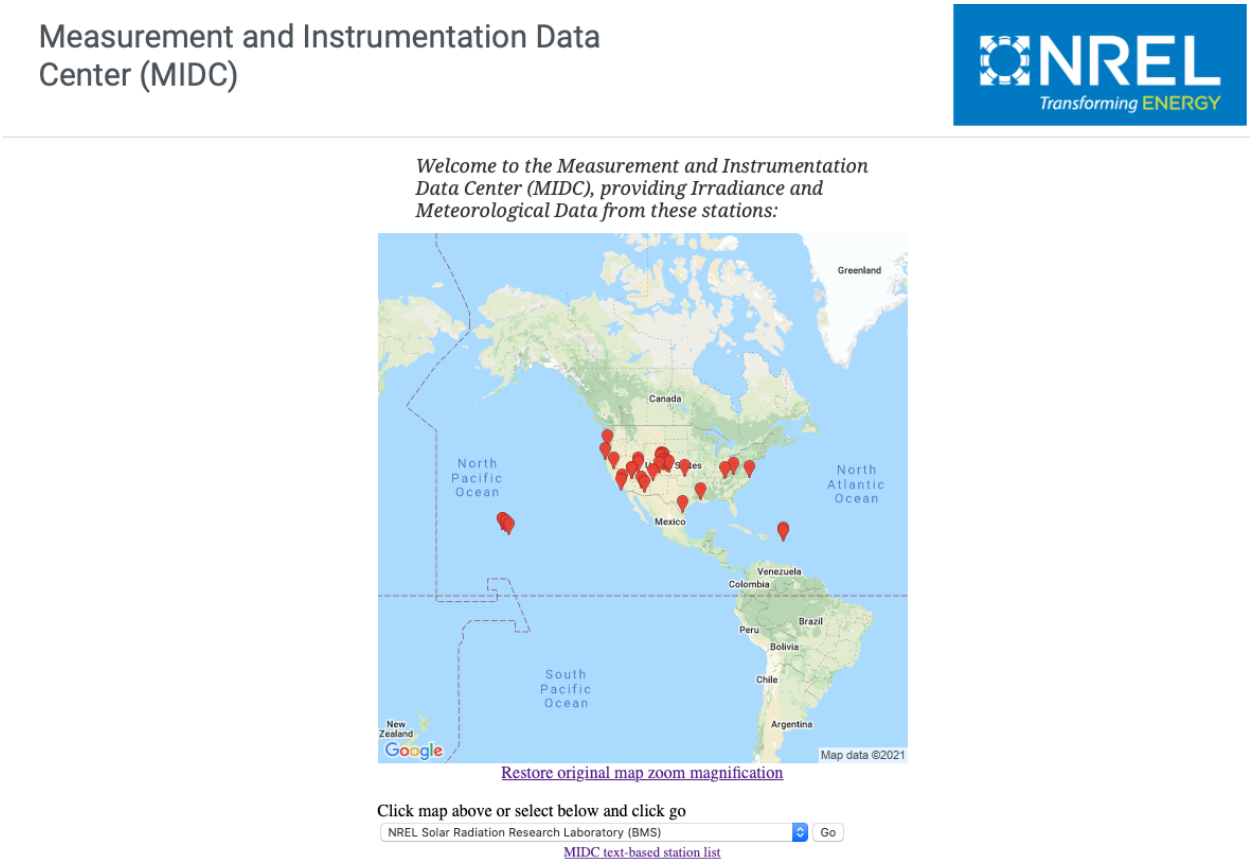

Figure 16. NREL MIDC station map

NREL keeps track of visits to the MIDC website that provides access to the NREL-SRRL data. Figure 17 shows user statistics for the MIDC and the grid modernization web page that holds archived solar resource data and solar resource models.[5]

[5] See https://www.nrel.gov/grid/solar-resource/renewable-resource-data.html.

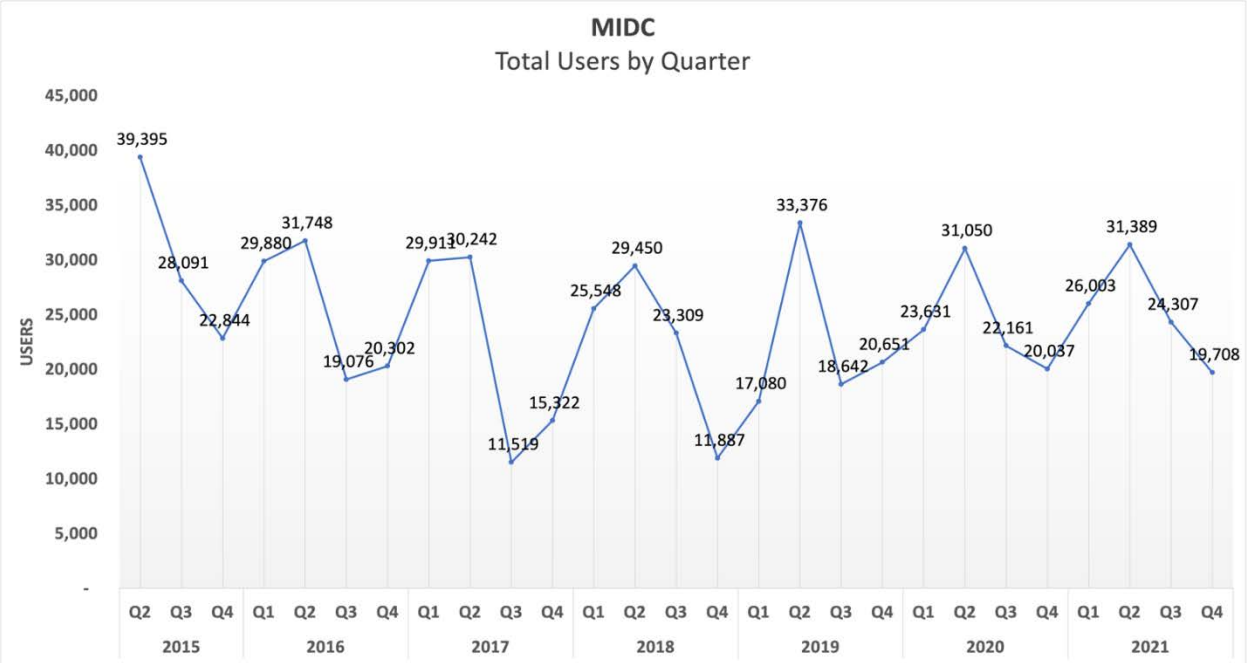

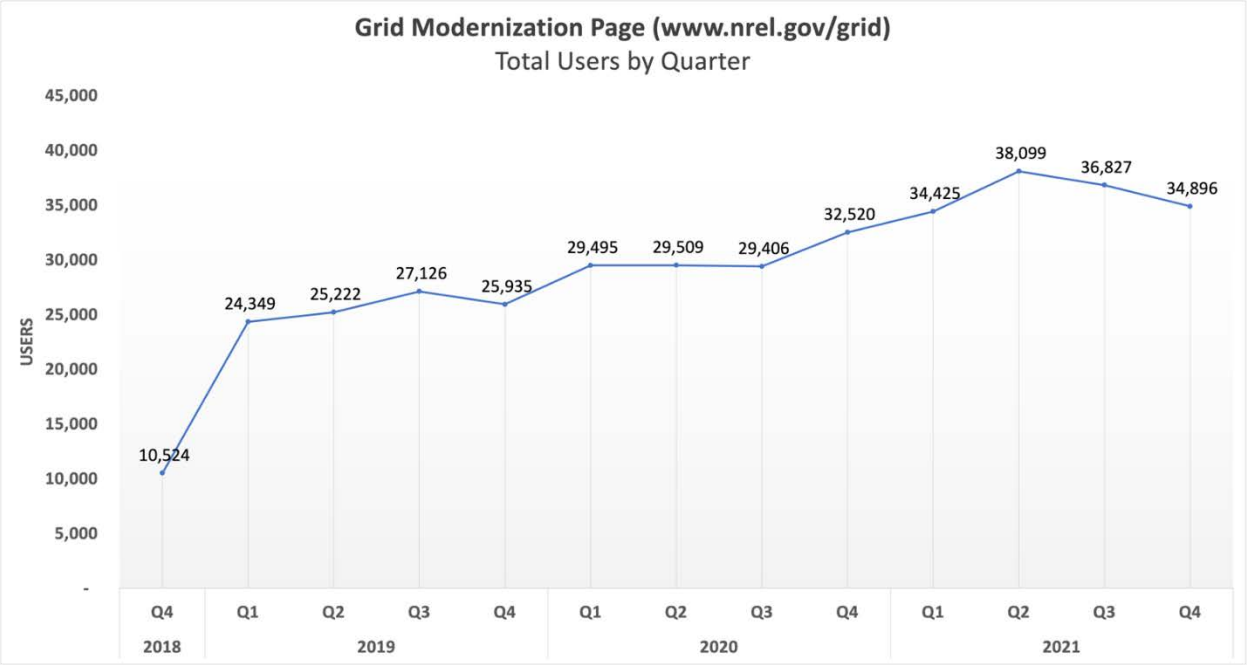

Figure 17. (Top) Quarterly MIDC user analytics and (bottom) accessed solar resource data and solar resource models under NREL's grid modernization web page

Further, NREL has been submitting BMS data to the World Radiation Data Center (WRDC), which publishes surface radiation data collected from the world radiometric network. The WRDC is a recognized World Data Center sponsored by the World Meteorological Organization. The WRDC centrally collects and archives radiometric data from around the world to ensure the availability of these data for research by the international scientific community. The WRDC issues the publication "Solar Radiation and Radiation Balance Data (The World

Network)" with the purpose of providing the users with data on solar radiation, radiation balance, and sunshine duration in a convenient and readily accessible form.

3.2 Task 2: Standards Development and Knowledge Sharing

A lack of common terminology, common methods, or awareness of national or international best practices, can lead to over- or underestimates of the available resource and long-term performance of a given solar power facility with higher uncertainty than warranted. These problems can result in over- or undersized equipment, increased financing costs, or poor plant financial performance. Standardization of data sets and models enables industry to develop widely accepted protocols for various stages of solar project development and operations. This reduces barriers to financing and reduces warranty costs. NREL developed and regularly updates the Best Practices Handbook for the Collection and Use of Solar Resource Data for Solar Energy Applications. This task supports NREL leadership in standards, best practices, and their timely dissemination to the U.S. solar energy industry, including manufacturers and developers (Figure 18).

There were two subtasks under this task.

1. Lead and contribute to the development and update of standards under ASTM and ISO.
2. Lead and contribute to activities under IEA PVPS Task 16.

Source: Habte, Sengupta, and Gueymard 2020

Figure 18. Standards, activities, and their applications

3.2.1 Develop, Update, and Disseminate Standards

NREL provided continued leadership in the development of standards that are relevant to the measurement and modeling of solar radiation for solar energy applications. Some of these standard bodies include the ASTM Subcommittee G03.09 on Radiometry, which is under the ASTM Committee G03: Weathering and Durability, and ISO TC 180/SC 1 Climate – Measurement and Data. The subcommittees promote knowledge and stimulate research on the calibration and specification of radiometers, the development of reference spectral irradiance, and radiometers' recommended field practices.

3.2.1.1 New Standards

- ASTM G222-21 – Standard Practice for Estimation of UV Irradiance Received by Field-Exposed Products as a Function of Location.[6] The scope of this standard describes the method to estimate the total solar ultraviolet irradiance on a horizontal surface as a function of air mass and geographic location. The standard provides a model for calculating global horizontal ultraviolet irradiance from GHI data for a specific location.
- CIE 241:2020 – Recommended Reference Solar Spectra for Industrial Applications.[7] The document details recommended reference solar spectra for total, direct, and diffuse components under various atmospheric conditions and solar geometries.

3.2.1.2 Standards Balloted and Reapproved During FY 2019–FY 2021

- ASTM G207-11(2019)e1 – Standard Test Method for Indoor Transfer of Calibration from Reference to Field Pyranometers
- ASTM G130-12(2020) – Standard Test Method for Calibration of Narrow- and Broad-Band Ultraviolet Radiometers Using a Spectroradiometer
- ASTM G138-12(2020)e1 – Standard Test Method for Calibration of a Spectroradiometer Using a Standard Source of Irradiance
- ASTM G173-03(2020) – Standard Tables for Reference Solar Spectral Irradiances: Direct Normal and Hemispherical on 37° Tilted Surface
- ASTM G177-03(2020) – Standard Tables for Reference Solar Ultraviolet Spectral Distributions: Hemispherical on 37° Tilted Surface
- ASTM G197-14(2021) – Standard Table for Reference Solar Spectral Distributions: Direct and Diffuse on 20° Tilted and Vertical Surfaces
- ASTM G222-21 – Standard Practice for Estimation of UV Irradiance Received by Field-Exposed Products as a Function of Location
- ASTM G169 - 01(2021) – Standard Guide for Application of Basic Statistical Methods to Weathering Tests
- ASTM G141 - 09(2021) – Standard Guide for Addressing Variability in Exposure Testing of Nonmetallic Materials.
- ISO/PRF TR 9901 Solar Energy – Pyranometers – Recommended Practice for Use.

3.2.1.3 Standards Balloted and Under Revision

- ISO/CD 9847 Solar Energy – Calibration of Pyranometers by Comparison to a Reference Pyranometer
- ISO/CD 9845-1 Solar Energy – Reference Solar Spectral Irradiance at the Ground at Different Receiving Conditions – Part 1: Direct Normal and Hemispherical Solar Irradiance for Air Mass 1.5
- ASTM WK38983 – New Guide for Performance Classification of Solar Radiometers.

---

[6] See https://www.astm.org/Standards/G222.htm.
[7] See https://cie.co.at/publications/recommended-reference-solar-spectra-industrial-applications.

3.2.2 Update of Solar Resource for Solar Energy Applications Handbook

Solar energy is fast becoming a major contributor to power production for many utilities around the world; however, data to understand and plan for this massively abundant energy resource is not always straightforward because the state of the art in solar resource data continually evolves and adopts advanced techniques. To help stakeholders stay abreast of the latest in solar resource data, the NREL, in collaboration with IEA PVPS Task 16 and SolarPACES technology programs published the third edition of the *Best Practices Handbook for the Collection and Use of Solar Resource Data for Solar Energy Applications*.[8]

The handbook covers the rapid evolution in the field of solar resource assessment and forecasting for solar energy applications. This handbook comprehensively describes the state of the field and serves as a reference document to stakeholders ranging from science to solar energy professionals and in solar applications that span concentrating solar power, PV, daylighting, and solar heating and cooling.

The rapid growth of the PV industry—in both the size of the installations and the penetration levels—boosted the need for accurate solar data for planning and operation. Similarly, during this rapid growth, significant enhancements in the knowledge of solar resource assessment and forecasting were attained, which are now included in this handbook. Distinct from past editions of the handbook, the third edition also features a new chapter on relevant meteorological parameters, such as wind, temperature, aerosols, and others. Another distinct focus in this edition was on the increasing importance of artificial intelligence applied to forecasts.

By helping solar stakeholders understand the nature of solar radiation, its variation around the world, and its evolution over time, this handbook contributes to making solar energy more predictable and more easily integrated into our energy systems.

3.3 Task 3: Reference Cell Calibrations and Spectral Measurement and Modeling for Photovoltaic Applications

Reference cell calibrations are provided by manufacturers, but they are calibrated indoors or outdoors using IEC 60904-4, and the calibration is only valid for normal incidence. The goal of this effort is to expand the validity of calibrations through developing new methods/processes similar to those used for NREL's ISO-accredited BORCAL process, which considers all angles of incidence.

3.3.1 Calibrations of Reference Cells Using Global Measurements

The objective of this subtask is as follows:

- Develop outdoor calibration method for reference cells using the NREL's BORCAL method.
- Acquire and use temperature correction equation and coefficients from NREL's Cell and Module Characterization Lab.

[8] See https://www.nrel.gov/docs/fy21osti/77635.pdf.

- Use spectral radiometer measurements and IEC/ASTM G173 standard reference spectra for spectral mismatch correction estimates.

NREL, PV Performance Labs, and the University of Oregon worked together to accomplish the planned objectives. PV Performance Labs, under a subcontract, delivered reports and submitted a journal paper that discussed the calibration comparisons between indoor and outdoor methods and the characterization of PV reference cells. One deliverable was titled *PV Reference Cells for Outdoor Use: An Investigation of Calibration Factors* and compares calibration factors from the manufacturer, NREL's Cell Lab, and BORCAL for many commercially available reference cells.[9] The study analyzed 39 reference cells that were obtained from 6 different manufacturers in the United States, United Kingdom, and Germany (Table 5). These reference cells differ in design, including size and type of cells, style and materials of the enclosure, mounting method, temperature sensing, and electrical interface. Nevertheless, most used monocrystalline silicon cells laminated under nontextured, low-iron float glass. Several polycrystalline cells were also included to investigate to what extent these might perform differently, whereas the filtered cell from Atonometrics and the amorphous cell from IKS Photovoltaik were included to see whether they offer any unique benefits. These reference cells are grouped by the letters P (polycrystalline), F (filtered), and A (amorphous), respectively, where relevant. Note: Four of these models were evaluated in a previous study (Driesse and Zaaiman 2015), which provides insight into the reproducibility of the result.

Table 5. Types of Reference Cells Used in This Study

Company	Model	ID	Type/ Designation	Fixed Tilt	Single Axis	Dual Axis
Atonometrics	810226-02	RC18	Mono	Yes	Yes	Yes
Atonometrics	810226-03	RC18	Filtered (for CdTe)/"F"			Yes
EETS	RC01	RC01	Mono	Yes	Yes	Yes
Fraunhofer ISE	511311102	WPVS	Mono	Yes		Yes
IKS Photovoltaik	ISET	ISET	Mono	Yes	Yes	Yes
IKS Photovoltaik	ISET-aSi	ISET	Amorphous/"A"	Yes		
IKS Photovoltaik	ISET-poly	ISET-P	Poly/"P"	Yes		
IMT	Si-mV-85-PT1000	Si2	Mono	Yes	Yes	Yes
NES	SOZ-03	SOZ-03	Mono	Yes	Yes	Yes
NES	SOZ-03-P	SOZ-03-P	Poly/"P"	Yes		

[9] See https://www.nrel.gov/docs/fy21osti/80437.pdf.

Comparing the NREL Cell Lab and the factory calibration factors showed that the monocrystalline calibrations were, on average, 0.8% higher than the Cell Lab. The two monocrystalline outliers were World Photovoltaic Scale (WPVS) cells from Fraunhofer ISE that were found to be 0.6% and 1.0% lower than those from the NREL Cell Lab; however, even with the bias, all these differences fall within the range of expectations. That is, the NREL calibrations have an uncertainty of approximately 0.9% (k=2), and the other manufacturers quote uncertainties ranging from 1.4%–3.0%.

For the non-monocrystalline cells, the largest observed differences were from amorphous cells, "A," from IKS that were higher by +6.6% and +9.3% (Figure 19). For these cells, the factory calibration was performed in 2012; therefore, some of the differences could be attributed to the instability of the calibration factors since the last calibration date. The pair of filtered monocrystalline cells, "F," from Atonometrics demonstrated the second highest differences, which could be related to how the references were calibrated in the factory. The manufacturer's certificate states that the filtered monocrystalline reference cells were calibrated outdoors using a monocrystalline cell as a reference, and this approach could possibly create a spectral mismatch between the reference device and the unit under calibration. The two IKS polycrystalline cells, "P," demonstrated smaller differences and were in the same range of differences as the IKS monocrystalline cells. Furthermore, most of reference cell calibrations, regardless of type, were positively biased with respect to the Cell Lab.

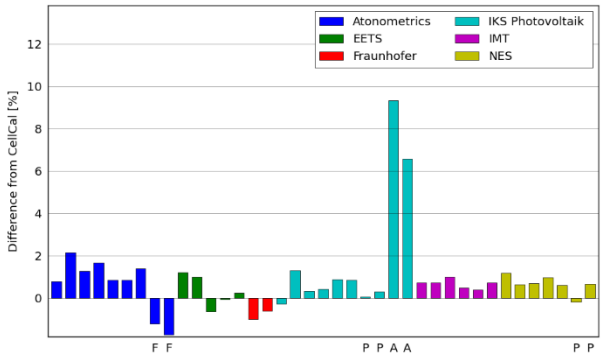

Figure 19. Differences in factory calibration factors from NREL's Cell Lab calibrations (unmarked: monocrystalline, F: filtered, P: polycrystalline, A: amorphous)

The short-circuit current (*Isc*) of PV cells, and therefore the irradiance signal of reference cells, is primarily caused by the decrease in bandgap energy with increasing temperature that broadens the spectral response toward the infrared (Osterwald et al. 2015). For most practical applications, this observed change in current with temperature, dI_{sc}/dT (typically referred to as α or TC), can be considered constant, although over a full range of operating conditions, the TC can vary up to 20% for a given sky condition (i.e., spectral distributions of incident irradiance) and varying spectral responsivity of the cell due to temperature and cell type.

Salis et al. (2019) reported that the uncertainty associated with the I_{sc} temperature coefficient measurements is significant, which affects the uncertainty of the TC. As shown in Figure 20, there are large differences between the reported specifications from the manufacturer and those from the Cell Lab-measured TC for the filtered cells, "F," and the polycrystalline cells, "P." For

example, “F” demonstrated negative measured coefficients reported by the manufacturer, but they were positive in the NREL Cell Lab.

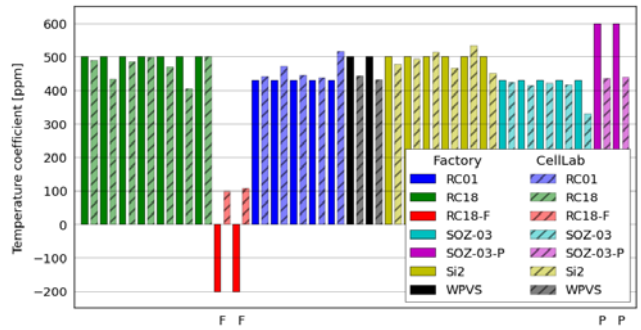

Figure 20. Comparison of factory temperature coefficients to those determined by NREL’s Cell Lab

Overall, the temperature correction (TCOR) of the reference cell output as used in this work was calculated using Eq. 8:

$$TCOR = 1 + (TC * (T_{cell} - 25)) \qquad \text{Eq. 8}$$

where T_{cell} is the measured temperature of each device (or an adjacent unit of the same type).

3.3.2 Measurement and Data Capabilities

The objective of this subtask was to deploy reference cells in multiple locations with different climatology for evaluating measurements using high-quality broadband measurements with thermopile radiometers. The deployment took place at both NREL and University of Oregon locations that were equipped with spectral radiometer and thermopile radiometers. (Figure 21 shows the NREL deployment setup.)

This subtask performed the following list of calibration and measurement activities:

1. Calibrated all thermopiles, spectral radiometers, and reference cells
2. Collected data for horizontal, fixed-tilt, one-axis, and two-axis tracking systems at NREL
3. Continued measurement of one-axis spectral, reference cell, and thermopile measurements at the University of Oregon
4. Collected and distributed spectral and reference cell measurement information through the MIDC for the NREL and University of Oregon sites
5. Distributed hourly spectral data from the NSRDB for 1998–2020.

Figure 21. (Top left) Two-axis trackers, (top right) one-axis trackers, and (bottom) fixed tilt with multiple instrumentations deployed at NREL-SRRL

3.3.3 Modeling and Validation

The objective of this subtask was to analyze measurements at NREL to accurately characterize the angle of incidence (AOI) and spectral effects using measurements from one-axis, two-axis, fixed-tilt, and horizontal systems.

PV Performance Labs and the NREL-SRRL team continued the characterization of PV reference cells. As a background, as stated in ASTM E2848-13(2018), reference cells are well suited for acceptance testing of newly installed PV systems. The irradiance obtained from reference cells reduces the uncertainty of the acceptance testing result. The standard recommends understanding and possibly quantifying the uncertainty introduced to the reference cell from such causes as spectral, directional, and temperature response errors; therefore, the study attempted to understand, quantify, and demonstrate the various sources of uncertainties of reference cell data. To accomplish this, the study developed reference data for comparison purposes using a weighted mean of the sensor values. The highest weights were assigned to the sensors that qualitatively had the fewest and smallest deviations during a preliminary comparison with the median. This turned out to be effective for illustrating differences but otherwise remains an imperfect reference. A percentage deviation statistic metric was calculated for the filtered data and the result is presented as follows using two types of charts:

1. A sun path diagram where the deviation metrics were binned by sun azimuth in 2.5° increments and by sun elevation in 1° increments, and the median value in each bin is

coded in color. The color scale was stepped so that a numeric value can be determined easily with a precision of 0.5% ranging from ±2.5%.

2. A time chart where the result showed a colored point representing the cell temperature for the percentage deviation of every measurement. The vertical range was expanded to ±10% to show extremes that are hidden from view by the median in the sun path diagram.

Using these metrics and charts, the result hereafter shows the directional, spectral, and temperature response analysis as well as the nonlinearity. The directional response analysis was focused on the fixed-tilt (latitude-tilt) orientation because the effect of this is moderate to minimum for the one-axis and two-axis tracking orientations, respectively. In the sun path diagram (Figure 22), the horizon created by the fixed-tilt POI (AOI = 90°) is drawn with a double line. The other double line is the geographic horizon, showing mountains to the south and west. The sun path diagram in Figure 22 shows IMT Si2, which has a very abrupt drop in irradiance response just before the sun sets on the horizon of the tilted plane. The cause for this appears to be the raised edge of the enclosure that partly shades the cell at very high incidence angles.

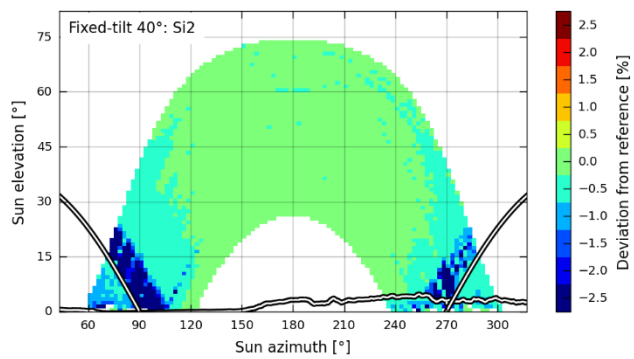

Figure 22. Effect of raised edge on IMT Si2

A very different pattern with a substantial asymmetry is shown in Figure 23. In the morning, the EETS RC01 has an enhanced response, especially near the tilted plane horizon, whereas in the evening, its response is somewhat lower than the reference data.

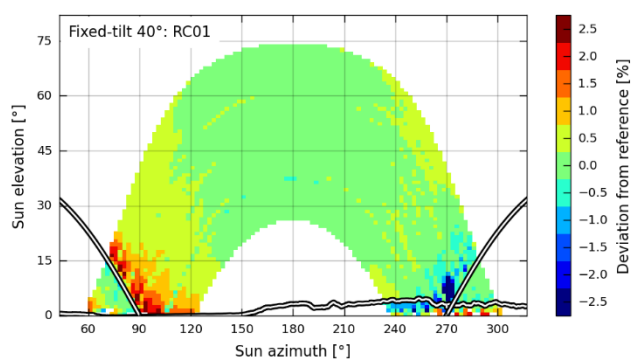

Figure 23. Effect of asymmetric white border on EETS RC01

The University of Oregon and the NREL-SRRL team performed a similar study approaching the characterization of PV reference cells from the modeling perspective to model reference cell

output using spectral and temperature data. An enhanced model was developed that incorporates the average AOI factor from beam, diffuse, and ground-reflected irradiance (Figure 24).

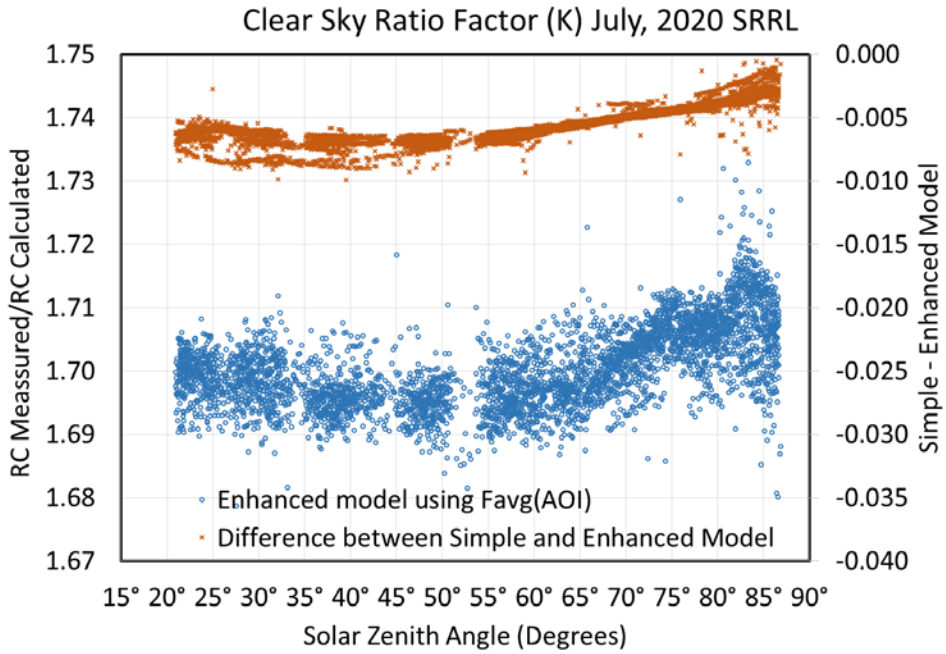

Figure 24. The relationship between the measured irradiance and the modeled reference cell measurement

The first approach of this study was published in *Solar Energy*, titled "Improved Field Evaluation of Reference Cells Using Spectral Measurements" (Vignola et al. 2020). The study analyzed the output from an IMT reference solar cell mounted on a one-axis tracking surface using spectral measurements covering the range from 350 nm–1650 nm for selected days throughout the year. Comparisons are made to a Class A pyranometer also mounted on the one-axis tracking surface. Systematic biases over the day and year were observed in the ratio of the reference cell measurements to the reference pyranometer measurements. This systematic bias is associated with the spectral, temperature, and AOI effects that differ between the reference cell and the reference pyranometer (Figure 25). The comparison was done for selected clear and totally cloudy days to determine the magnitude of the effects and to characterize the influence of these effects on the reference cell measurements. A model to calculate the reference cell output based on spectral irradiance and reference cell temperature was introduced.

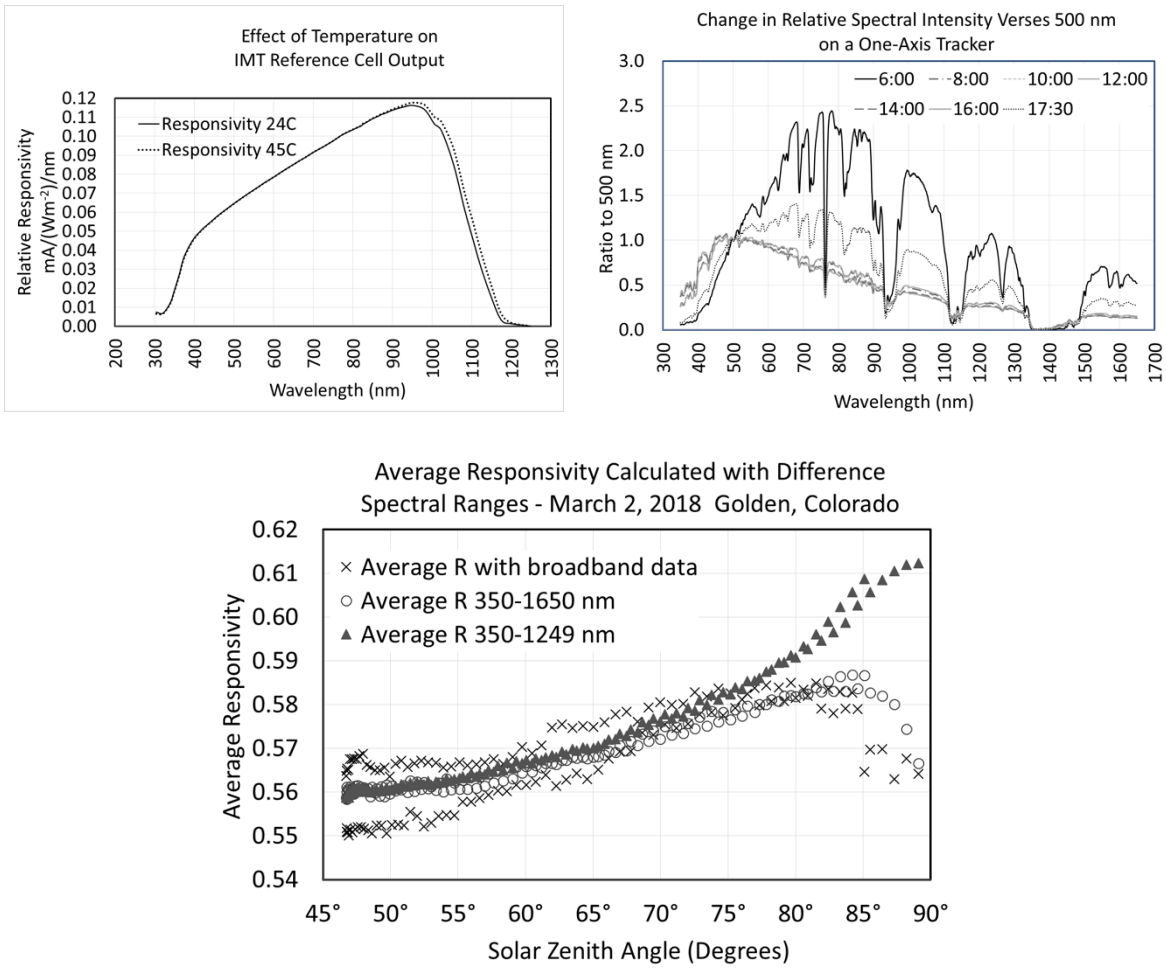

Figure 25. (Top left) Relative spectral responsivity of an IMT mono-silicon reference cell. Measurements were made at 24ºC and 45ºC under a NIST-calibrated lamp. (Top right) Relative change in clear-sky spectral intensity at different times of the day normalized to one at 500 nm on September 13, 2018. Early morning (6:00— solar zenith angle = 87°) and late afternoon (17:30— solar zenith angle = 82.5°) exhibit a dramatic shift in the spectral distribution from distributions during the middle of the day. (Bottom) Comparison of average responsivity calculated with wavelengths from 350 nm–1249 nm, wavelengths from 350 nm–1650 nm, and the use of broadband data for the denominator. The three sets of average R values are set equal at 47°.

The modeled reference cell output (RC) for is proportional the sum of the spectral and temperature dependence of the reference cell $R(I_\lambda,T_\lambda)$ times the spectral irradiance I_λ times transmission of the irradiance through the glazing F(AOI), see Eq. 9.

$$RC = K \cdot \sum_{280nm}^{4000nm} R(I_\lambda, T_\lambda) \cdot I_\lambda \cdot F(AOI) \qquad \text{Eq. 9}$$

where K is similar to a responsivity that relates the measured current or voltage to the total irradiance, λ is the wavelength, and T_λ is the spectral temperature sensitivity of the reference cell. The values of $R(I_\lambda,T_\lambda)$ are determined from the normalized quantum efficiency of the reference cell determined using a solar lamp at the NREL laboratory. To simplify the calculation, the

transmission of light through the glazing, *F(AOI)*, was assumed to be independent of the wavelength. When pulling *F(AOI)* out of the sum over wavelengths in Eq. 9, the integrated reference cell responsivity times the spectral responsivity, $\bar{R}$, was obtained.

To test the postulated relationship IMT measurements the *K* ratio values were determined by dividing the measured IMT values by *F(AOI)* times $\bar{R}$.

$$K = IMT/(F(AOI) \cdot \bar{R}) \qquad \text{Eq. 10}$$

The more consistent the *K* value is over all solar angle and types of irradiance, the more comprehensive the postulated relationship.

To minimize the influence of the angle of incidence, the data collected on a two-axis tracking surface were studied. For the beam irradiance, the sensors would be perpendicular to the incident radiation and *F(AOI)* would be 1. *F(AOI)* for the various diffuse components were less than one and when included in the calculations, a more consistent *K* value was obtained. The irradiance on the two-axis tracker was broken down into the beam and diffuse components using the Perez model (Perez et. al, 1990) and the transmission of diffuse light through the glazing, *F(AOI)*s, was calculated using the Marion model (Marion, 2017).

The study found that under clear sky conditions that the *K* factor for the IMT reference cell was approximately 1.70 ± 0.02 at a 95% level of confidence in July and December. Under totally cloudy conditions, *K* was 1.70 ± 0.07 in July and 1.69 ± 0.08 in December. It was found that modeling the *F(AOI)* for the diffuse components shifted the results by several percent and were necessary to obtain a consistent *K* value over the clear and cloudy conditions and over the year (see Figure 26). For a more detailed discussion see Vignola, et. al, 2021.

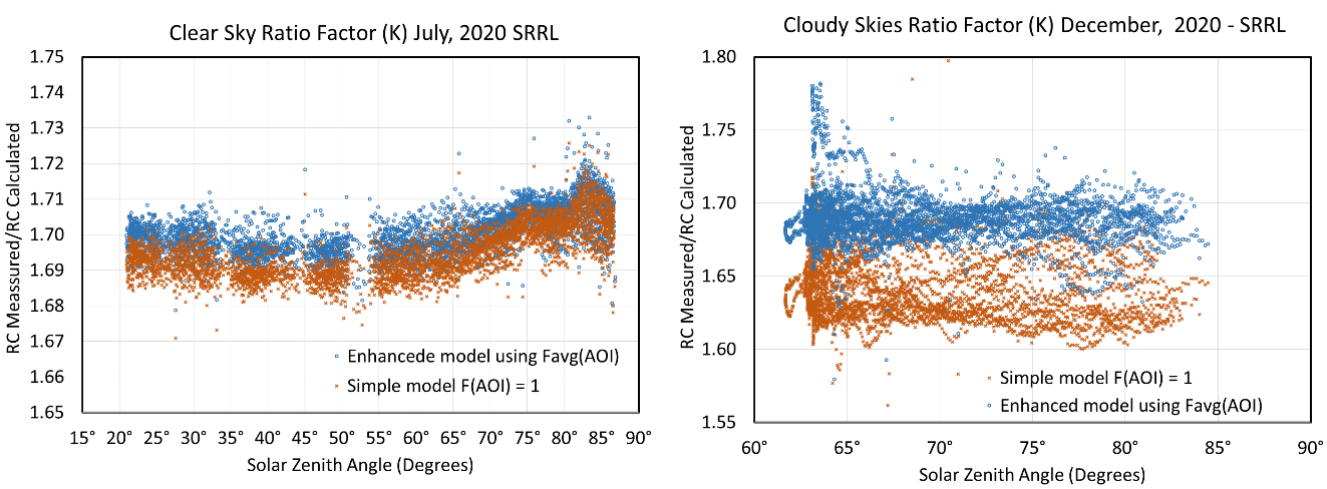

Figure 26: Plots of the ratio of the measured IMT output compared with the calculated IMT output in July 2020 under clear skies and in December 2020 under totally cloudy skies at the NREL-SRRL in Golden, Colorado. Examples show the value of using the *F(AOI)* calculated modeling the diffuse transmission of light through the glazing.

3.3.3.1 National Solar Radiation Database Spectral and Measured Spectral Comparison

A recent effort by NREL led to a new radiative transfer model, the Fast All-Sky Radiation Model for Solar Applications with Narrowband Irradiances on Tilted surfaces (FARMS-NIT), to efficiently compute spectral irradiances in the POA. This model has been implemented in the NSRDB to provide PV resource in both narrowband and broadband wavelengths. A study was conducted to evaluate the spectral irradiances from the PV resource data set using surface-based observations at the NREL-SRRL and the University of Oregon. The results demonstrate that the PV resource has a generally good agreement with the long-term observations in both clear-sky and cloudy-sky conditions. Further research is needed to reduce the overestimation of visible irradiances in clear-sky conditions and the underestimation of near-infrared irradiances in cloudy-sky conditions.

In this study, the spectral irradiances from the PV resource data were evaluated using surface-based observations at the NREL-SRRL and the University of Oregon. For the NREL-SRRL, the spectral irradiances were measured by a horizontal EKO WISER spectroradiometer system consisting of a set of instruments, such as the MS-711 and the MS-712. The spectral data on the horizontal surface were given at 1-nm intervals ranging from 350 nm–1650 nm. For the University of Oregon, the spectral data were measured by a MS-711 mounted on a one-axis tracking system to cover 1-nm intervals ranging from 300 nm–1100 nm.

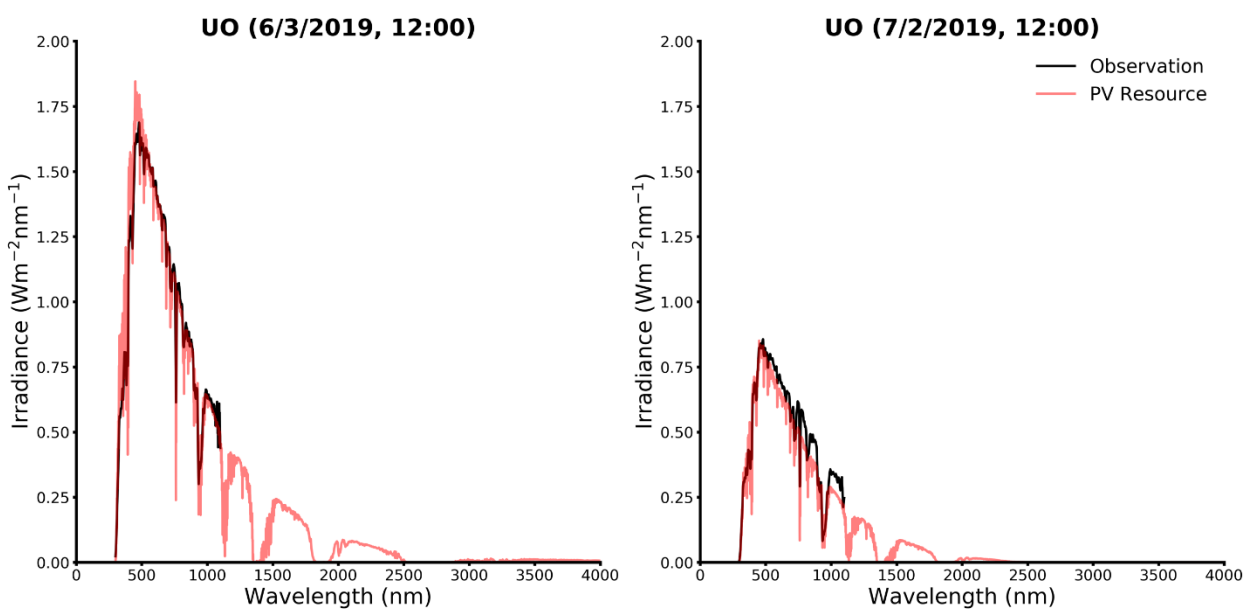

Figure 27. A comparison of spectral irradiances on a (left) clear-sky and a (right) cloudy-sky scene at the University of Oregon

Note that any data point is not exact, and there are uncertainties associated with the data. Even if the data do match, there is still uncertainty in the data, and the match can only be as good as the data or model. Still, it always builds confidence in the model for the modeled and measured data match, even if there are systematic uncertainties and biases in the measured data. It is useful to look at clear-sky and cloudy-sky conditions over the year to see how well models and data match. Figures 27 and 28 illustrate the spectral irradiances at NREL-SRRL and the University of Oregon, respectively. The curve of the measured data is smoother than that of the modeled data

because the measurements by the spectroradiometers are recorded at 1-nm separations, and the spectral model data are recorded at smaller wavelength intervals. More importantly, the measured data at a given wavelength also include measurements from other nearby wavelengths because the spectroradiometer has an average full width at half maximum of less than 7 nm. This has the effect of averaging over a range of wavelengths. If the full width at half maximum is a Gaussian distribution and is consistent over all wavelengths, the effect of this spread can be calculated; however, without actual laboratory tests, it is difficult to address this issue in a comprehensive manner. The spectroradiometer also has a directional response that is better than 5% for the MS-711. This can affect any comparison. On the one-axis tracker, the spectroradiometer is pointing more toward the sun and should have minimal directional effects; however, that must be proven. Figures 27 and 28 show that the clear-sky irradiances from the PV resource data are underestimated in the visible wavelengths, whereas a much better agreement can be found in the near-infrared wavelengths. This probably indicates an underestimation of the transmittance of the aerosol. For cloudy-sky conditions, however, the spectral irradiances from the PV resource data are underestimated. At specific wavelengths, e.g., 950 nm, the modeled and measured data can be considerably different. This is caused by the spectral measurements having a full width at half maximum of 7 nm or less; therefore, the measurement at a given wavelength is a combination of measurements from the surrounding wavelengths as well as at the given wavelength.

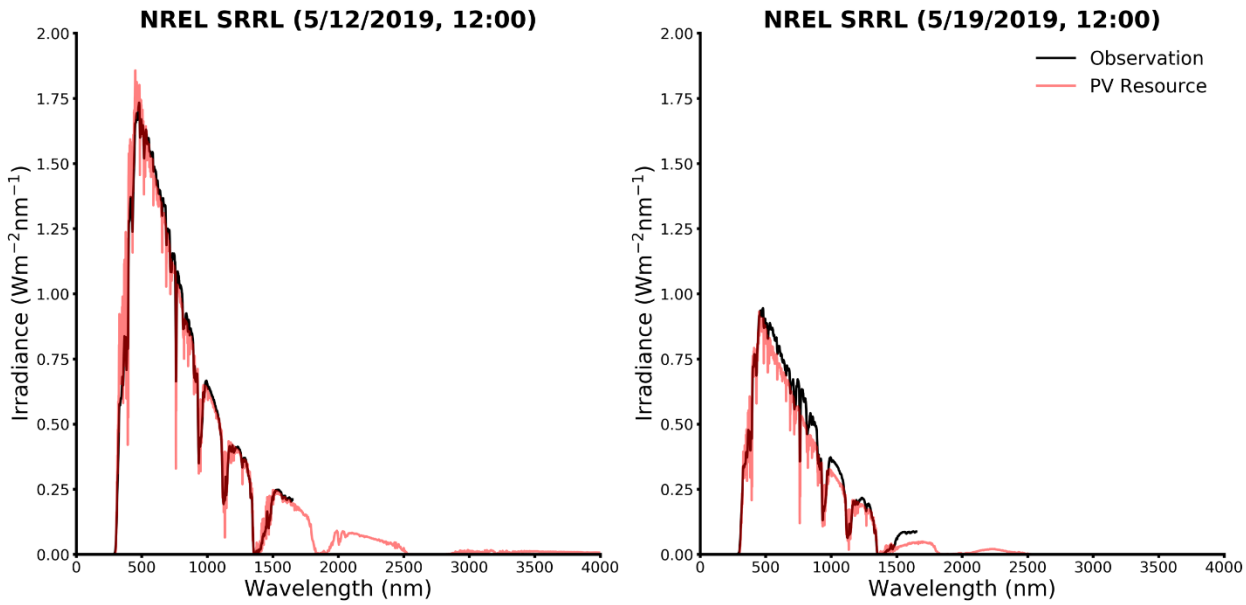

Figure 28. A comparison of spectral irradiances on a (left) clear-sky and a (right) cloudy-sky scene at NREL-SRRL

It can be concluded that the PV resource data have a generally good agreement with the long-term observations; however, some differences are noticeable. The clear-sky irradiances at visible wavelengths are underestimated by the PV resource data. This is probably caused by the uncertainty in the aerosol optical depths at the wavelengths. On the other hand, the cloudy-sky irradiances at near-infrared wavelengths are slightly overestimated by the PV resource data. Larger differences between the PV resource data and the surface observations can be seen at specific wavelengths that are particularly sensitive to water vapor absorption. This can be related to the relatively coarse wavelength resolution in the observations as well as the influence from

the surrounding wavelengths. Moreover, some of the differences observed could also be attributed to the uncertainty of the spectroradiometers.

3.3.3.1.1 Evaluation of Photovoltaic Resource Data from the NSRDB

In our previous work supported by this project, we developed a comprehensive capability to provide spectrally resolved PV resource data from the NSRDB, effectively providing 20 years of hourly data for the contiguous United States at a 4-km by 4-km spatial resolution. We integrated the advantages of the current models and developed an innovative radiative transfer model, FARMS-NIT, to efficiently compute irradiances on inclined PV panels for 2002 narrow-wavelength bands from 0.28 µm–4.0 µm. For clear-sky conditions, the Simple Model of the Atmospheric Radiative Transfer of Sunshine (SMARTS) (Gueymard 1995) was employed to rapidly provide the optical properties of a given clear-sky atmosphere. The clear-sky radiances in the narrow-wavelength bands were computed by considering three paths of photon transmission and solving the radiative transfer equation with the single-scattering approximation. The bidirectional transmittance distribution function of aerosols was given by their single-scattering phase function with a correction using a two-stream approximation. For cloudy-sky conditions, FARMS-NIT uses cloud reflectance of irradiance and the bidirectional transmittance distribution function from a precomputed lookup table by the libRadtran model with a 32-stream Discrete Ordinates Radiative Transfer (DISORT) (Stamnes et al. 1988). The cloud reflectance and bidirectional transmittance distribution function are combined with the clear-sky properties to efficiently compute spectral radiances on the land surface and POA irradiances.

These data are now available free to users directly through a geographic information system-based web interface[10] as well as through an application programming interface (Sengupta et al. 2018; Xie and Sengupta 2018; Xie, Sengupta, and Dooraghi 2018; Xie, Sengupta, and Dudhia 2016). Users of these data can conduct more accurate prefeasibility studies and assess multiple PV technologies. To promote the use of the PV resource data by widely used models—such as PVSyst; NREL's System Advisor Model (SAM) (Blair et al. 2014); and PlantPredict, designed by First Solar—it is important to understand the performance and accuracy of the data as evaluated by surface-based observations. In this quarter, we analyzed long-term observations (2013–2018) from six surface sites operated by the First Solar to evaluate the PV resource data provided by the NSRDB. Figure 29 illustrates the locations of the surface sites at Picture Rocks, Arizona; Neenach, California; Deming, New Mexico; Calipatria, California; and London, Ontario (Canada). Note that the blue spots represent the availability of fixed-tilt observations, and the red spots represent measurements from one-axis tracking systems. The green spots indicate that both fixed-tilt and one-axis tracking observations are available (see more site information in Table 6). The GHI is measured by all sites using a number of Kipp & Zonen CMP11 pyranometers.

Figure 30 compares GHI between surface observations and PV resource data from the NSRDB. The blue bands represent the variations in the surface observations from different pyranometers. It is clear that the PV resource data have reasonable agreement over all sites under both clear-sky and cloudy-sky conditions; however, the 30-minute resolution PV resource data are insufficient to represent the rapid variations in solar radiation, as shown in the 1-minute observations (e.g., in

[10] See https://nsrdb.nrel.gov.

Figures 30d and 30f). This bias should be reduced using the next generation of satellite data with an improved temporal resolution. Further, the observational uncertainty from different instruments might affect the accuracy of the evaluation, as shown in Figure 30b.

Figure 31 compares the long-term GHI from surface observations and PV resource data. The 1-minute measurements of GHI are averaged over each hour and compared with the PV resource data for the surface sites. The GHI data from the PV resource all have a decent performance over time. The MBE, MAE, percentage error, and absolute percentage error (APE) for the sites are given in Table 7. The magnitudes of the error metrics are comparable to those reported in Sengupta et al. (2018). For the surface sites with more clouds (e.g., Site 5 and Site 6), the MBE and MAE are lower than the other sites; however, they have relatively larger percentage errors and APEs due to the increased uncertainty in computing cloudy-sky radiation.

Table 6. Site Information on the Six First Solar Ground Stations

Site No.	Location	Latitude (°N)	Longitude (°W)	Time	CMP11 (horizontal)	CMP11 (fixed tilt)	CMP11 (1-axis)	RC (fixed tilt)	RC (1-axis)	Tilt Angle (°)
1	Picture Rocks, AZ	32.371533	111.282784	1/1/2013-12/31/2018	4	0	4	0	9	1-axis tracking
2	Neenach, CA	34.778913	118.427015	2/1/2013-12/31/2018	5	5	0	3	0	25
				7/1/2014-12/31/2018	10	0	10	0	3	1-axis tracking
3	Deming, NM	32.572799	107.486525	6/1/2014-12/31/2018	2	0	2	0	4	1-axis tracking
4	Calipatria, CA	33.171175	115.448442	12/1/2014-12/31/2018	2	0	2	0	5	1-axis tracking
5	Sarnia, Canada	42.935169	82.335933	10/1/2010-12/31/2017	6	6	0	17	0	25
6	London, Canada	42.891388	81.11028	2/1/2013-12/31/2018	2	2	0	5	0	25

Table 7. MBE, MAE, Percentage Error, and APE of GHI from the PV Resource Data in the NSRDB

	MBE ($Wm^{-2}\mu m^{-1}$)	MAE ($Wm^{-2}\mu m^{-1}$)	PE (%)	APE (%)
Site 1	22.38	51.5	5.17	11.91
Site 2	21.19	48.03	4.9	11.1
Site 3	21.32	56.27	5.41	14.27
Site 4	19.76	41.15	5.18	10.8
Site 5	10.9	34	6.85	21.38
Site 6	10.6	63.99	3.71	22.38

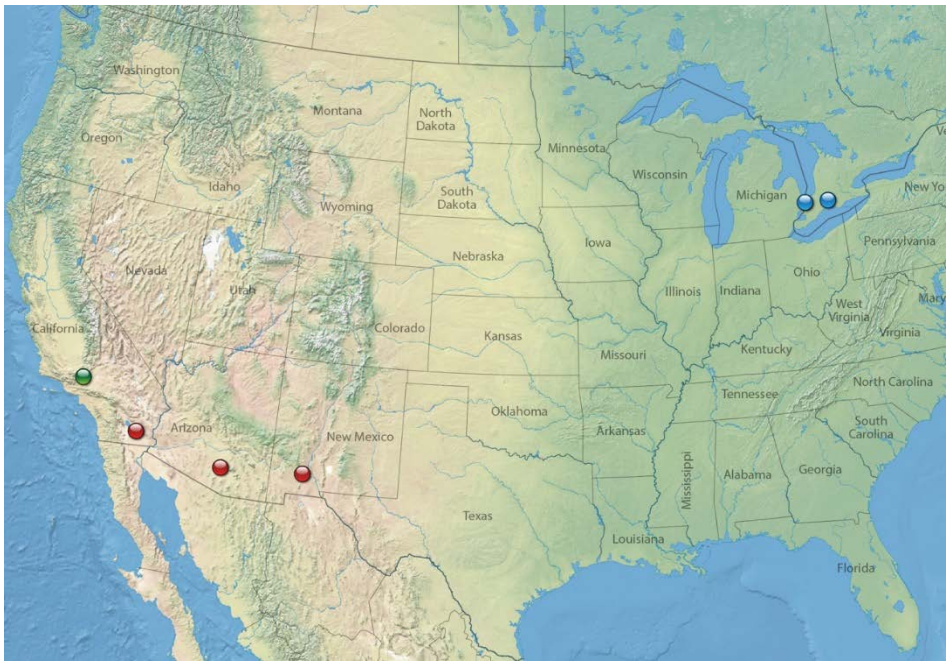

Figure 29. The location of the six surface sites used in the evaluation. The blue spots represent that observations from fixed-tilt surfaces are available. The red spots represent that those from one-axis trackers are available. The green spots indicate that both fixed-tilt and one-axis tracking observations are available.

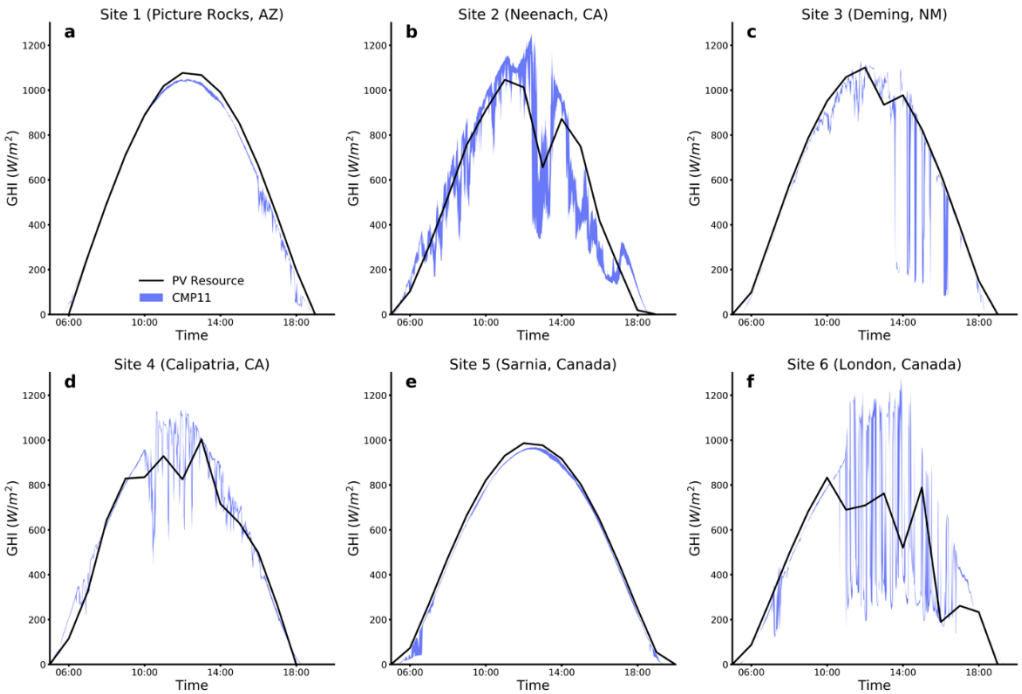

Figure 30. Comparison of GHI between surface observations and PV resource data from the NSRDB on May 1, 2015

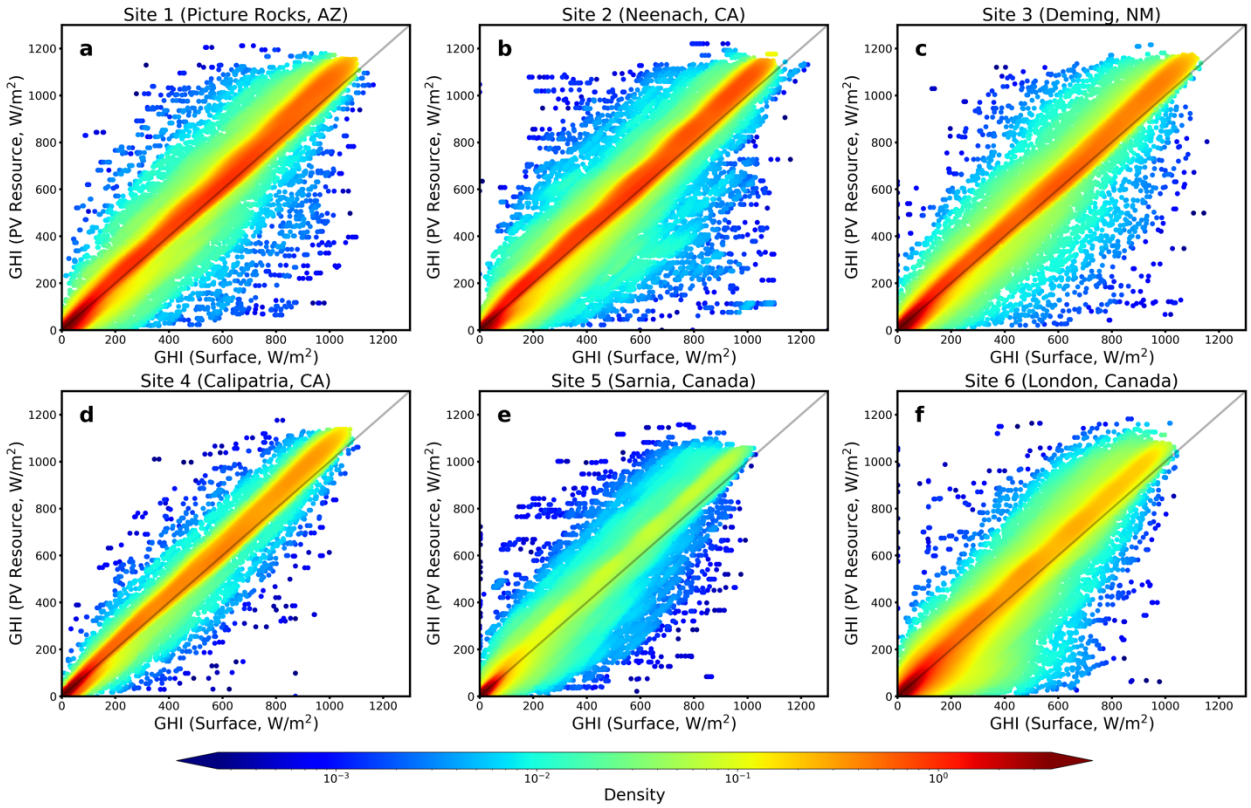

Figure 31. Comparison of long-term GHI from surface observations and PV resource data

3.3.3.1.2 Evaluation of Reference Cells by Comparison to Thermopile

Solar radiation is routinely measured or computed on horizontal surfaces; however, for greater solar energy gain, PV modules are often inclined with respect to the horizontal plane to reduce the solar incident angle. In contrast to PV modules with fixed-tilt angles, they can also be mounted on a solar tracking system, either rotating along a single axis or having two degrees of freedom to more closely follow the sun's daily east-west motion as well as the seasonal north-south motion. The global solar irradiance reaching the inclined PV modules are often referred to as POA irradiance.

POA irradiance in system performance simulations is usually computed by transposition models using surface-based observations of GHI and DNI. In this study, we investigate a transposition model developed by Perez et al. (1987) that has been extensively used in solar energy applications (hereafter referred to as the Perez model). This model uses a modified form of the isotropic diffuse radiation on the PV plane to consider the enhanced solar radiation around the circumsolar region. The main equations of the model are given as functions of solar zenith angle, horizontal diffuse irradiance, and direct radiation, where the coefficients of the questions are empirically determined using hourly observations from Trappes and Carpentras, France. Although only 2-year POA irradiances observed by a 45° south-facing plane and vertical planes facing east, south, west, and north were used in developing the model, it shows acceptable accuracy at multiple locations and plane orientations.

The POA irradiance measured by PV modules suffers from an energy reduction caused by the reflection by the glass surface covering the PV modules. According to Snell's law and the Fresnel equations, the energy reduction can be derived by the effective reflectivity of unpolarized light as a function of the refractive index of the glass and the solar incident angle. With the assumption of infinitely narrow direct solar radiation, the derivation of the AOI correction factor for direct radiation is straightforward; however, the computation for diffuse radiation can be extremely complicated resulted from the solar radiances from multiple directions with various intensities. Marion (2017) significantly simplified this computation by assuming that the diffuse radiation is isotropic. With the assumption, the AOI correction factor can be given by an integral of differential AOI correction factors associated with the solid angles in the field of view. This approach was used to compute the AOI correction factors for two different types of glass surfaces: the uncoated glass (n = 1.526) and the antireflection-coated glass (n = 1.3).

To examine the transposition models and measurement of POA irradiance by reference cell, we collected 1-minute resolution observations by a CMP22 thermopile and an IMT reference cell on a one-axis tracking system at NREL-SRRL. For the model simulation, the 1-minute surface pressure and GHI data observed by a horizontal CMP22 were also collected in 2019. Figure 32 is a flowchart of computing the POA irradiances and comparing them with surface observations. The surface-measured GHI were first applied to the Direct Insolation Simulation Code (DISC) (Maxwell 1987) to compute DNI. The GHI and DNI were then used by the Perez transposition model to numerically calculate the POA irradiance for a PV module on a one-axis tracking system. The POA irradiance was observed by the IMT reference cell. Following the numerical model reported by Marion (2017), the energy reduction by the PV surface reflection was considered by using the AOI correction factors for diffuse radiation associated with uncoated and antireflection-coated glass. The model simulation and corrected observation were compared with the observation from the CMP22 thermopile on the one-axis tracker.

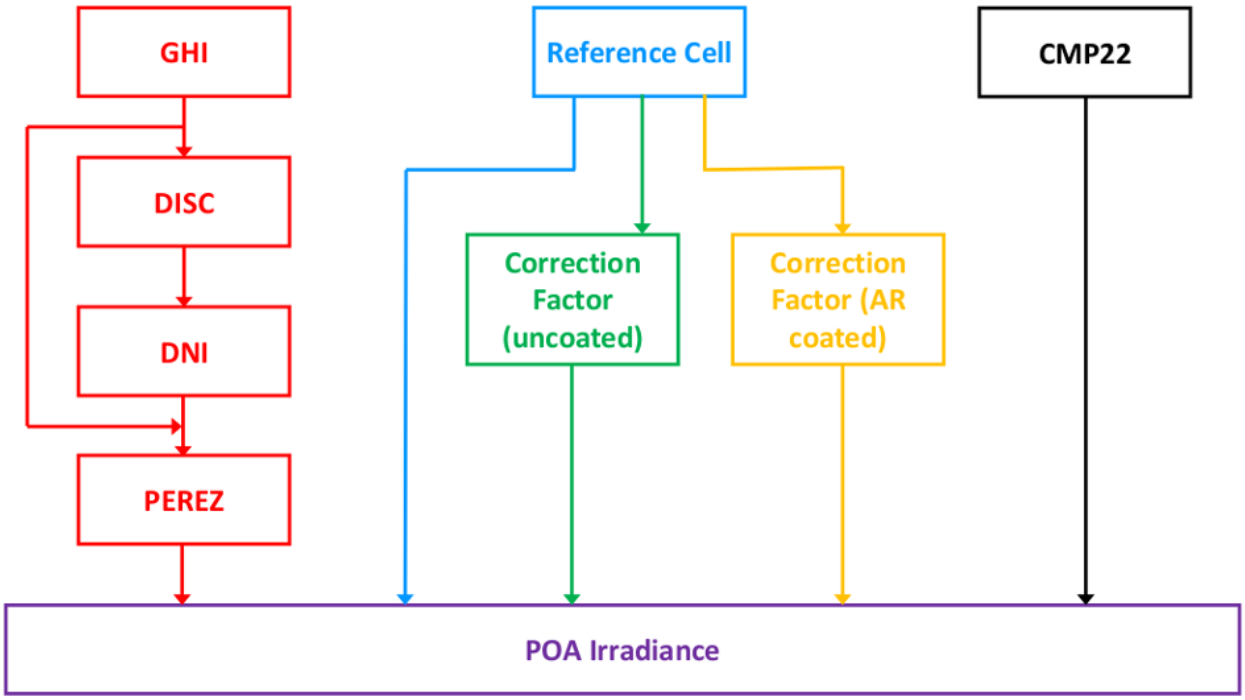

Figure 32. Flowchart for POA comparison

Figure 33 compares the POA irradiances from the model simulation and observation. Compared to the IMT data in the selected 4 days, the computation from the Perez model has greater deviation from the more precise observation by the CMP22, especially in cloudy-sky conditions. Also, the IMT observation without a correction of the PV surface reflection underestimates the POA irradiance. The underestimation becomes more obvious at noon than the other times because the PV surface reflection is determined by the solar incident angle and the magnitude of the POA irradiance. With the correction of the PV surface reflection, the energy reduction is moderated, whereas the correction factor for the antireflection-coated glass leads to even smaller bias.

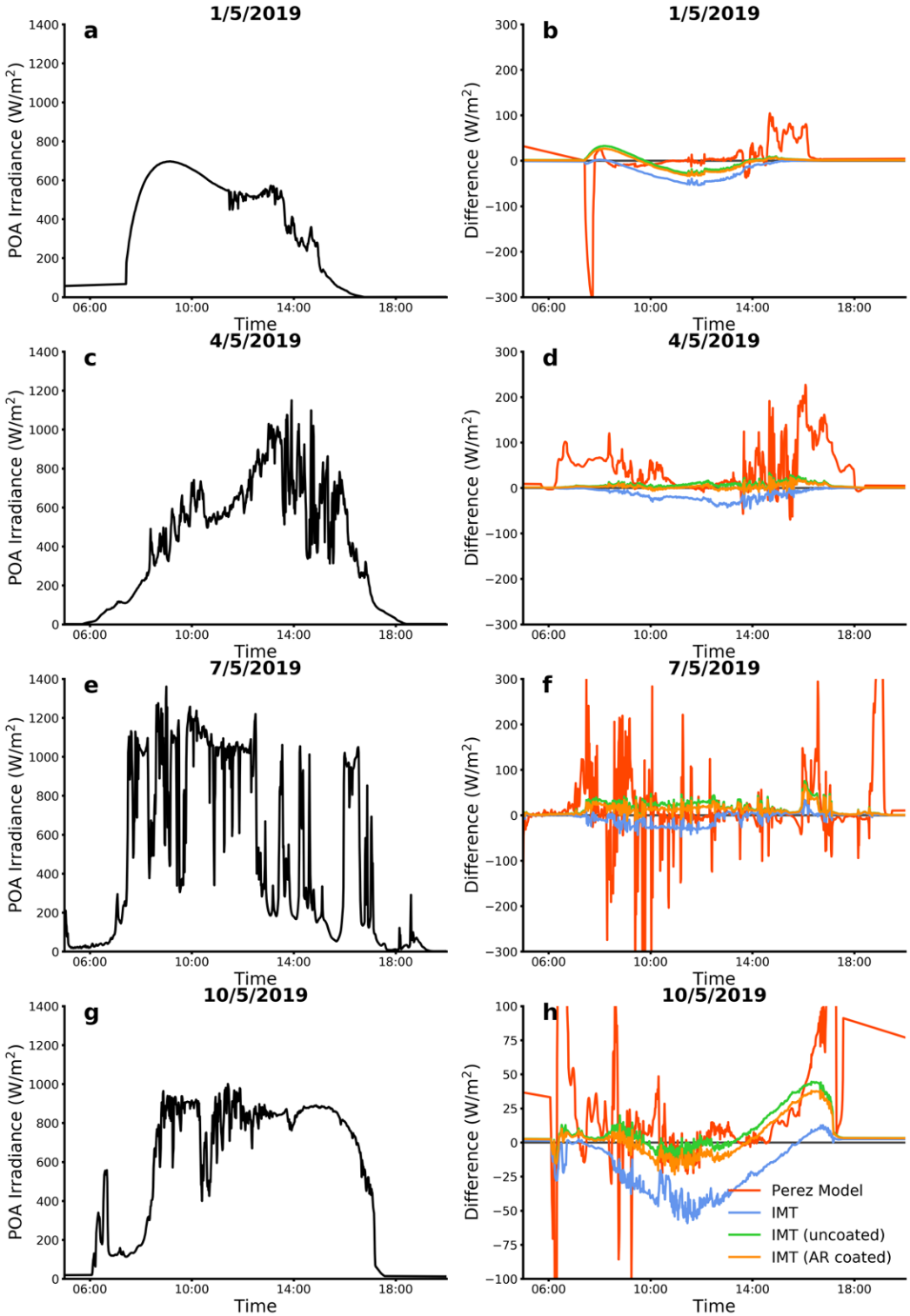

Figure 33. Daily solar energy comparison for selected days in 2019

The consequence is consistent in long-term data, as shown in Figure 34, where the daily solar energy are compared over 2019. The annual POA irradiances for the thermopile (Kipp & Zonen

CMP22), the thermopile POA through the Perez decomposition model, the PV reference cell (IMT), the IMT (uncoated), and the IMT (antireflection coated) are 2323, 2393, 2269, 2375, 2355 kWh/m^2, respectively. The 1-minute resolution data from the model simulation and IMT measurements are compared with the CMP22 in Figure 35, where the green line represents the regression of the data. Based on the MBE, MAE, percentage error, and APE, the Perez model slightly overestimates the POA irradiance and leads to a greater deviation from the CMP22 measurements. The correction factors for the PV surface reflection effectively reduce the measurement uncertainty from the IMT reference cell. The correction factor related to the antireflection-coated glass reduces the IMT measurement error by approximately 50% according to the MBE and percentage error values.

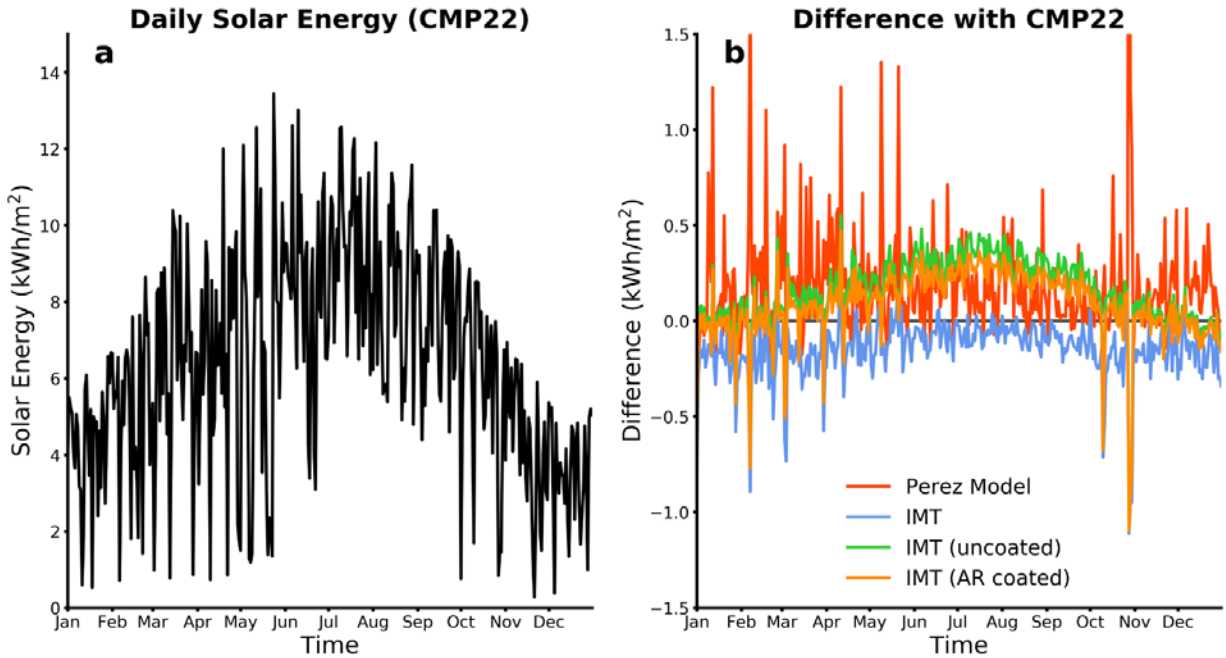

Figure 34. POA irradiance comparison from the model simulation and observation

A technical report was published[11] demonstrating that the NREL-calibrated reference cells have reduced uncertainty in estimated energy generation when compared to energy generation computed using GHI from a thermopile and converted to the same array orientation.

[11] See https://www.nrel.gov/docs/fy21osti/80260.pdf.

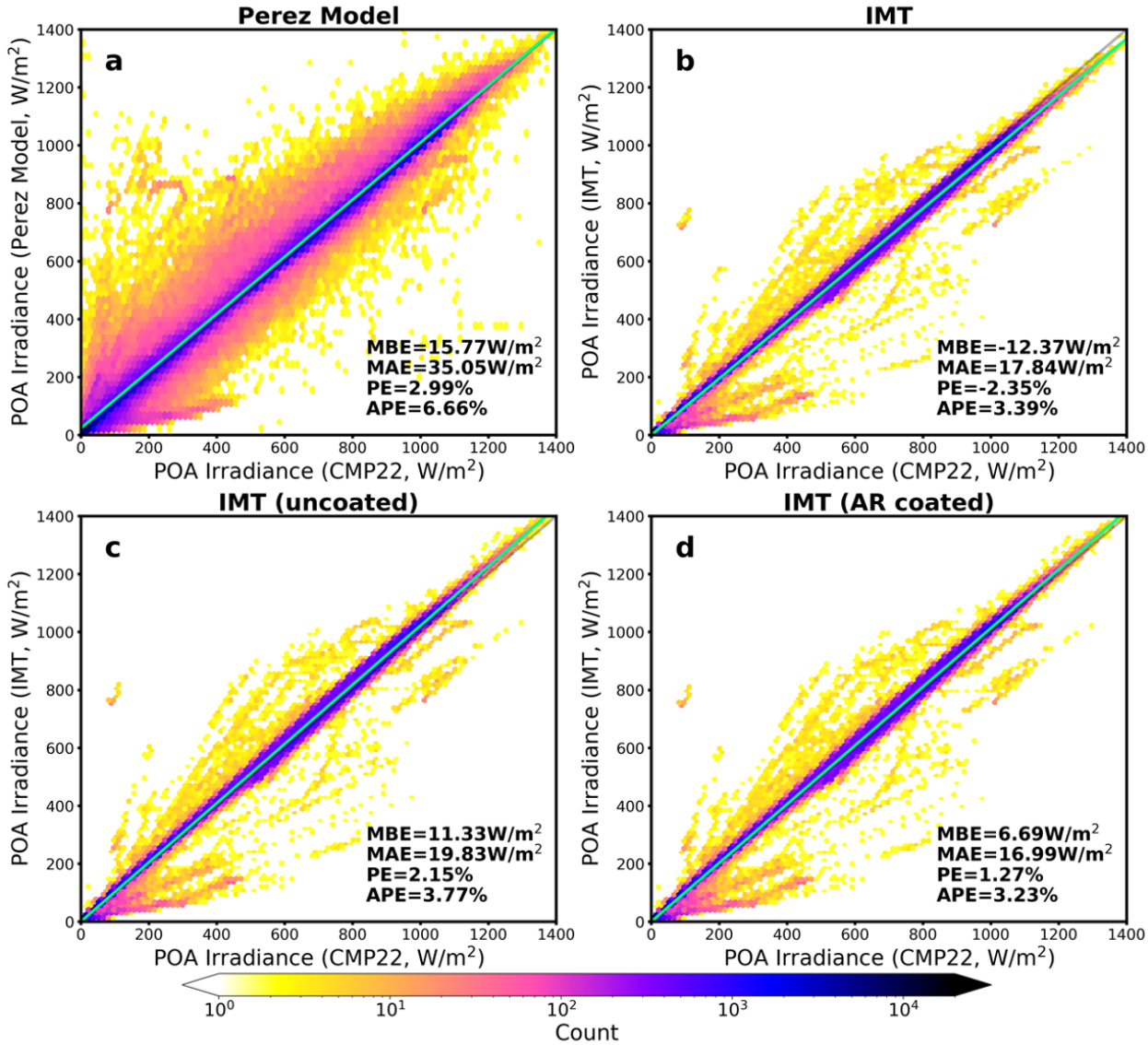

Figure 35. Comparison of 1-minute resolution data for one year from the model simulation and IMT measurements against the thermopile pyranometer CMP22. The green line represents the regression of the data.

4 Path Forward

The NREL-SRRL is an internationally recognized laboratory in solar resource measurements, calibration, and modeling. The NREL-SRRL will continue the work to support R&D projects supported by SETO—including PV performance and characterization, numerous economic and performance models, policy analysis, and grid integration systems—because accurate solar resource data are essential for reducing barriers to achieving SETO's goals. Further, for decades, DOE has invested millions of dollars in the SRRL and NREL to develop unique capabilities for providing world-class solar resource measurement and modeling techniques.

Therefore, the SRRL project at NREL will continue to provide calibration traceability to the WRR for reference radiometers used by DOE and numerous stakeholders participating in each NPC. Instruments deployed at NREL will be calibrated using the BORCAL facility or the Spectral Calibration Lab, thereby providing ISO-accredited calibrations to broadband and spectral radiometers for instruments that are deployed in the NREL BMS and providing research-quality data important for advancing solar resource characterization, solar resource modeling for various technologies, and the validation and verification of new models. Moreover, the project will seek to develop state-of-the-art instrumentation and methods that enable the adoption of new solar energy technologies. The NREL-SRRL will continue the long-standing leadership roles and involvement in international standardization through the ASTM, the ISO, the IEC, and the IEA. The NREL-SRRL will continue to deploy, develop, and characterize measurements of high accuracy from the BMS to enable advanced radiometry and solar modeling, to support industry to reduce the cost of solar project development, and to develop the capability to use low-cost measurements for effective grid integration.

One task that the NREL-SRRL will continue to perform in the next 3 years is on PV reference cells. In principle, a well-matched PV reference cell deployed near a PV plant in any geographic location will provide an accurate measurement of effective irradiance (the irradiance that is used by PV modules) over the full range of operating conditions: temperature, cloudiness, sun position, season, etc. This contrasts with broadband irradiance measurements from pyranometers, which must be processed using a variety of models to estimate effective irradiance. High-quality reference cell measurements can eliminate these modeling steps and thereby remove the models' contribution to uncertainty in various project planning and evaluation activities.

The advantage of measuring effective irradiance as opposed to modeling is particularly relevant for evaluating the contribution of reflected radiation to the performance of bifacial modules and systems. Both directional and spectral distributions of reflected radiation strongly differ from the front-side irradiance, and there are currently no practical models to translate rear-side pyranometer measurements into rear-side effective irradiance.

Two additional aspects are important for good reference cell measurements: accurate calibration and long-term stability. This is no different from any other measurement, but few studies have examined these qualities of commercial reference cells. Through this activity, the NREL-SRRL will provide stakeholders with state-of-the-art reference cell measurement approaches to measure effective irradiance, thereby removing the models' contribution to uncertainty in various project planning and evaluation activities.

Publications: Inventions, Patents, Publications, and Other Results

Fiscal Years 2019–2021 Publications

Book Chapters/Handbook

Rosseler, Olivier, Aron Habte, Manajit Sengupta, Christian A. Gueymard, and David M. Burns. 2020. "13 - A Simple Estimation of UV Irradiance Under Clear-Sky conditions." In *Plastics Design Library, Service Life Prediction of Polymers and Coatings*. William Andrew Applied Science Publishing, pages 257–266. ISBN 9780128183670. https://doi.org/10.1016/B978-0-12-818367-0.00013-8. (http://www.sciencedirect.com/science/article/pii/B9780128183670000138)

Sengupta, Manajit, Aron Habte, Stefan Wilbert, Christian Gueymard, and Jan Remund. 2021. *Best Practices Handbook for the Collection and Use of Solar Resource Data for Solar Energy Applications: Third Edition*. Golden, CO: National Renewable Energy Laboratory. NREL/TP-5D00-77635. https://www.nrel.gov/docs/fy21osti/77635.pdf.

Standard

Suga, S., P. Blattner, O. Cordo, G. Cornell, A. Francis, A. Habte, J. Jung, H. Kita, D. R. Myers, J. Regan, A. Schönlein, and A. Thorseth. 2020 Recommended Reference Solar Spectra for Industrial Applications. International Commission on Illumination (CIE). https://doi.org/10.25039/TR.241.2020.

Journal Articles

Forstinger, Anne, Stefan Wilbert, Anton Driesse, Natalie Hanrieder, Roman Affolter, Sharad Kumar, Neeraj Goswami, Norbert Geuder, Frank Vignola, Luis Zarzalejo, and Aron Habte. 2020. "Physically Based Correction of Systematic Errors of Rotating Shadowband Irradiometers." *Energy Meteorology* 29 (1): 19–39. https://www.nrel.gov/docs/fy20osti/77334.pdf.

Habte, A., M. Sengupta, C. A. Gueymard, R. Narasappa, O. Rosseler, and D. M. Burns. 2019. "Estimating Ultraviolet Radiation from Global Horizontal Irradiance." *IEEE Journal of Photovoltaics* 9 (1): 139–146. https://doi.org/10.1109/JPHOTOV.2018.2871780.

Hosseinian Ahangharnejhad, R., A. Phillips, K. Ghimire, P. Koirala, Z. Song, H. M. Barudi, A. Habte, M. Sengupta, R. J. Ellingson, Y. Yan, R. W. Collins, N. J. Podraza, and M. J. Heben. 2019. "Irradiance and Temperature Considerations in the Design and Deployment of High Annual Energy Yield Perovskite/CIGS Tandems." *Sustainable Energy and Fuels* 7. http://dx.doi.org/10.1039/C9SE00237E.

Miller, David C., Fahad Alharbi, Afshin Andreas, Jayesh G. Bokria, David M Burns, Jaynae Bushong, Xinxin Chen, Dennis Dietz, Sean Fowler, Xiaohong Gu, Aron Habte, Christian C. Honeker, Michael D. Kempe, Hussam Khonkar, Michael Köhl, Nancy H. Phillips, Jorge Rivera, Kurt P. Scott, Ashish Singh, and Allen F. Zielnik. 2020. "Degradation in Photovoltaic Encapsulation Strength of Attachment: Results of the first PVQAT TG5 Artificial Weathering Study. *Progress in Photovoltaics: Research and Applications*: 1–20. https://doi.org/10.1002/pip.3255.

Reda, Ibrahim, Afshin Andreas, Peter Gotseff, and Mark Kutchenreiter. 2020. "Using an Absolute Cavity Pyrgeometer to Validate the Calibration of a Secondary Standard Pyrgeometer Outdoors, Independent from the Reference Value of the Atmospheric Longwave Irradiance." *Atmospheric and Climate Sciences* 10 (4): 530–37. https://doi.org/10.4236/acs.2020.104027. https://www.nrel.gov/docs/fy20osti/77810.pdf.

Shaffery, Peter, Aron Habte, Marcos Netto, Afshin Andreas, and Venkat Krishnan. 2020. "Automated Construction of Clear-Sky Dictionary from All-Sky Imager Data." *Solar Energy* 212: 73–83. https://doi.org/10.1016/j.solener.2020.10.052.

Vignola, Frank, Josh Peterson, Richard Kessler, Vikram Sandhu, Sean Snider, Aron Habte, Peter Gotseff, Afshin Andreas, Manajit Sengupta, and Fotis Mavromatakis. 2021. "Improved Field Evaluation of Reference Cells Using Spectral Measurements." *Solar Energy* 215: 482–91. https://doi.org/10.1016/j.solener.2020.12.063.

Technical Reports

Dooraghi, Michael, Afshin Andreas, Mark Kutchenreiter, Ibrahim Reda, Martina Stoddard, Manajit Sengupta, and Aron Habte. 2019. *Broadband Outdoor Radiometer Calibration (BORCAL) Process for the Atmospheric Radiation Measurement (ARM) Program: Second Edition*. Golden, CO: National Renewable Energy Laboratory. NREL/TP-5D00-71476. https://www.nrel.gov/docs/fy19osti/71476.pdf. https://dx.doi.org/10.2172/1494284.

Driesse, Anton, Peter Gotseff, and Manajit Sengupta. 2021. *PV Reference Cells for Outdoor Use: An Investigation of Calibration Factors*. Golden, CO: National Renewable Energy Laboratory. NREL/TP-5D00-80437. https://www.nrel.gov/docs/fy21osti/80437.pdf.

Habte, Aron, Afshin Andreas, Manajit Sengupta, Ranganath Narasappa, Andy Hoke, Peter Gotseff, Ramanathan Thiagarajan, Adam Wolf, Loreli Carranza, and Danielle Watts. 2019. *Low-Cost Multiparameter Device for Solar Resource Applications*. Golden, CO: National Renewable Energy Laboratory. NREL/TP-5D00-73104. https://www.nrel.gov/docs/fy19osti/73104.pdf.

Reda, Ibrahim, Afshin Andreas, Aron Habte, Peter Gotseff, Mark Kutchenreiter, and Martina Stoddard. 2019. *NREL Pyrheliometer Comparisons: September 23–October 4, 2019 (NPC-2019)*. Golden, CO: National Renewable Energy Laboratory. NREL/TP-1900-75123. https://www.nrel.gov/docs/fy20osti/75123.pdf.

Sengupta, Manajit, Aron Habte, Yu Xie, Anthony Lopez, Mike Dooraghi, Mark Kutchenreiter, Afshin Andreas, Ibrahim Reda, Galen Maclaurin, Michael J. Foster, and Christian Gueymard. 2019. *Solar Resource Calibration, Measurement, and Dissemination: Final Report FY 2016–FY 2018*. Golden, CO: National Renewable Energy Laboratory. NREL/TP-5D00-73667. https://www.nrel.gov/docs/fy19osti/73667.pdf.

Sengupta, Manajit, Aron Habte, and Mike Dooraghi. 2019. *PV Variability at the DeSoto Next Generation Solar Energy Center: Cooperative Research and Development Final Report, CRADA Number CRD-11-425*. Golden, CO: National Renewable Energy Laboratory. NREL/TP-5D00-75427. https://www.nrel.gov/docs/fy20osti/75427.pdf.

Xie, Y., M. Sengupta, M. Dooraghi, and A. Habte. 2019. *Reducing PV Performance Uncertainty by Accurately Quantifying the PV Resource*. Golden, CO: National Renewable Energy Laboratory. NREL/TP-5D00-73377. https://www.nrel.gov/docs/fy19osti/73377.pdf.

Conference Papers

Gostein, Michael, Silvana Ayala Pelaez, Chris Deline, Aron Habte, Clifford W. Hansen, William F. Marion, Jeff Newmiller, Manajit Sengupta, Joshua S. Stein, and Itai Suez. 2021. "Measuring Irradiance for Bifacial PV Systems: Preprint." Presented at the 48th IEEE Photovoltaic Specialists Conference (PVSC 48), June 20–25, 2021. NREL/CP-5K00-80281. https://www.nrel.gov/docs/fy21osti/80281.pdf.

Habte, Aron, Manajit Sengupta, and Christian A. Gueymard. 2020. "Consensus International Solar Resource Standards and Best Practices Development: Preprint." Presented at the 47th IEEE Photovoltaic Specialists Conference (PVSC 47). June 15–August 21, 2020. NREL/CP-5D00-75879. https://www.nrel.gov/docs/fy20osti/75879.pdf.

Vignola, Frank, Josh Peterson, Rich Kessler, Aron Habte, Peter Gotseff, Manajit Sengupta, and Fotis Mavromatakis. 2020. "Using Spectral Measurements to Characterize Solar Reference Cells on a Two-Axis Tracker: Preprint." Presented at the 47th IEEE Photovoltaic Specialists Conference (PVSC-47), June 15–August 21, 2020. NREL/CP-5D00-76896. https://www.nrel.gov/docs/fy20osti/76896.pdf.

Vignola, Frank, Josh Peterson, Richard Kessler, Vikram Sandhu, Manajit Sengupta, and Aron Habte. 2019. "Improved Field Evaluation of Reference Cell Using Spectral Measurements: Preprint." Presented at the 46th IEEE Photovoltaic Specialists Conference (PVSC 46), Chicago, Illinois, June 16–21, 2019. NREL/CP-5D00-74037. https://www.nrel.gov/docs/fy19osti/74037.pdf.

Vignola, Frank, Josh Peterson, Fotis Mavromatakis, Stefan Wilbert, Anne Forstinger, Michael Dooraghi, and Manajit Sengupta. 2019. "Removing Biases from Rotating Shadowband Radiometers." AIP Conference Proceedings, Paper No. 190017. https://doi.org/10.1063/1.5117714

Wilbert, Stefan, Wilko Jessen, Anne Forstinger, Anton Driesse, Aron Habte, Manajit Sengupta, Aitor Marzo, Frank Vignola, and Luis F. Zarzalejo. "Application of the Clear-Sky Spectral Error for Radiometer Classification in ISO 9060: Preprint." Presented at the International Solar Energy Society (ISES) Solar World Congress, Santiago, Chile, November 4–7, 2019. NREL/CP-5D00-74454. https://www.nrel.gov/docs/fy20osti/74454.pdf.

Xie, Yu, and Manajit Sengupta. 2020. "Evaluation of the PV Resource Dataset in Central and North America: Preprint." Presented at the 37th European Photovoltaic Solar Energy Conference and Exhibition (EU PVSEC 2020), September 7–11, 2020. NREL/CP-5D00-77790. https://www.nrel.gov/docs/fy20osti/77790.pdf.

Conference Presentations/Posters

Habte, Aron, and Manajit Sengupta. 2020. "Modeling of Ultraviolet Irradiance from Total Irradiance: A Simplified Approach." Presented at the 2020 PV Reliability Workshop, February 25–27, 2020, Lakewood, Colorado.

Habte, Aron, and Manajit Sengupta. 2019. "Standards and Best Practices for Solar Measurements." Presented at the PV Systems Symposium, May 14–16, 2019. Albuquerque, New Mexico. https://www.nrel.gov/docs/fy19osti/73909.pdf.

Habte, Aron, Manajit Sengupta, Afshin Andreas, and Yu Xie. 2019. "Data Quality Assessment Using SERI-QC." 6th International Conference Energy & Meteorology (ICEM), June 24–27, 2019, Copenhagen, Denmark. https://www.nrel.gov/docs/fy19osti/74202.pdf.

Kutchenreiter, Mark, Aron Habte, Afshin Andreas, and Manajit Sengupta. 2019. "Ventilator Improvements for Reducing Radiometer Frost, Snow, and Ice Accumulation." Presented at the ARM/ASR PI Meeting, June 10–13, 2019, Rockville, Maryland. https://www.nrel.gov/docs/fy19osti/74105.pdf.

Reda, Ibrahim, Julian Grobner, Stefan Wacker, Christian Thomann, Afshin Andreas, Peter Gotseff, and Sengupta Manajit. 2020. "Results of Recent and Historical Comparisons Between Absolute Cavity Pyrgeometer (ACP), InfraRed Integrating Sphere (IRIS)." Presented at the 2020 – 16th BSRN Scientific Review and Workshop, June 29–July 3, 2020, Bologna, Italy. NREL/PR-1900-75896. https://www.nrel.gov/docs/fy20osti/75896.pdf.

Reda, Ibrahim, and Manajit Sengupta. 2019. "Establishing the World Reference for Measuring the Atmospheric Longwave Irradiance with Traceability to the International System of Units." Presented at the Joint ARM User Facility and ASR PI Meeting, Washington, D.C., June 10–13, 2019. https://www.nrel.gov/docs/fy19osti/73811.pdf.

Sengupta, Manajit, and Aron Habte. 2019. "Data Quality Assessment Using SERI-QC." Presented at the 6th International Conference Energy & Meteorology (ICEM), June 24–27 June 2019, Copenhagen, Denmark. https://www.nrel.gov/docs/fy19osti/74203.pdf.

References

Andreas, A., and S. Wilcox. 2016. *Radiometer Calibration and Characterization (RCC) User's Manual: Windows Version 4.0*. Golden, CO: National Renewable Energy Laboratory. NREL/TP-3B10-65844. https://doi.org/10.2172/1240772.

ASTM International. 2018. ASTM E2848-13(2018) – Standard Test Method for Reporting Photovoltaic Non-Concentrator System Performance. West Conshohocken, PA. www.astm.org.

Blair, N., A. Dobos, J. Freeman, T. Neises, M. Wagner, T. Ferguson, P. Gilman, and S. Janzou. 2014. *System Advisor Model, SAM 2014.1.14: General Description*. Golden, CO: National Renewable Energy Laboratory. NREL/TP-6A20-61019. Accessed October 31, 2016. https://www.nrel.gov/docs/fy14osti/61019.pdf.

Driesse, A., and W. Zaaiman. 2015. "Characterization of Global Irradiance Sensors for Use with PV Systems." Presented at the 2015 IEEE 42nd Photovoltaic Specialist Conference (PVSC), 1–5. https://doi.org/10.1109/PVSC.2015.7356004.

Dutton, E. G., J. J. Michalsky, T. Stoffel, B. W. Forgan, J. Hickey, D. W. Nelson, T. L. Alberta, and I. Reda. 2001. "Measurement of Broadband Diffuse Solar Irradiance Using Current Commercial Instrumentation with a Correction for Thermal Offset Errors." *Journal of Atmospheric Oceanic Technology* 18, 297–314. https://doi.org/10.1175/1520-0426(2001)018%3C0297:MOBDSI%3E2.0.CO;2.

Ekhosuehi, N., and E. Dickson. 2016. "On Forecast Performance Using a Class of Weighted Moving Average Processes for Time series." Journal of Natural Sciences Research 6 (13). Accessed March 28, 2021. https://iiste.org/Journals/index.php/JNSR/article/view/31793

Fröhlich, C. 1991. "History of Solar Radiometry and the World Radiation Reference." *Metrologia* 28: 111–15.

Grewal M. S. 2011. "Kalman Filtering." In International Encyclopedia of Statistical Science, edited by M. Lovric. Berlin, Heidelberg: Springer. https://doi.org/10.1007/978-3-642-04898-2_321.

Gueymard, C. 1995. *SMARTS2: A Simple Model of the Atmospheric Radiative Transfer of Sunshine: Algorithms and Performance Assessment*. Cocoa, FL: Florida Solar Energy Center.

Habte, A., M. Sengupta, A. Andreas, I. Reda, and J. Robinson. 2017. "Radiometer Calibration Methods and Resulting Irradiance Differences." *Progress in Photovoltaics: Research and Applications* 25: 614–22. https://doi.org/10.1002/pip.2812.

Habte, A., M. Sengupta, A. Andreas, S. Wilcox, and T. Stoffel. 2016. "Intercomparison of 51 Radiometers for Determining Global Horizontal Irradiance and Direct Normal Irradiance Measurements." *Solar Energy* 133: 372–93.

Habte, A., M. Sengupta, and C. A. Gueymard. 2020. "Consensus International Solar Resource Standards and Best Practices Development: Preprint." Presented at the 47th IEEE Photovoltaic Specialists Conference (PVSC 47), June 15–August 21, 2020. NREL/CP-5D00-75879. https://www.nrel.gov/docs/fy20osti/75879.pdf.

Harvey, A. 1990. Forecasting, Structural Time Series Models and the Kalman Filter. Cambridge: Cambridge University Press. https://doi.org/10.1017/CBO9781107049994.

International Electrotechnical Commission (IEC). 2019. IEC 60904-4:2019: Photovoltaic Devices—Part 4: Reference Solar Devices: Procedures for Establishing Calibration Traceability. Geneva, Switzerland.

Johnston, F., J. Boyland, M. Meadows, et al. 1999. "Some Properties of a Simple Moving Average When Applied to Forecasting a Time Series." Journal of the Operational Research Society 50: 1,267–71. https://doi.org/10.1057/palgrave.jors.2600823.

Lyche, T., and L. L. Schumaker. 1973. "On the Convergence of Cubic Interpolating Splines." In Spline Functions and Approximation Theory, edited by A. Meir and A. Sharma, 169–189. Birkhäuser.

Marion, B., 2017. Numerical method for angle-of-incidence correction factors for diffuse radiation incident photovoltaic modules, Solar Energy 147 (2017) 344–348

Marion, B., et al. 2017. "A Practical Irradiance Model for Bifacial PV Modules." Presented at the 44th IEEE Photovoltaic Specialists Conference (PVSC), Washington, D.C.

Maxwell, E. 1987. "A Quasi-Physical Model for Converting Hourly Global Horizontal to Direct Normal Insolation." Presented at the Solar Energy Research Institute, Golden, Colorado.

Maxwell, E., S. Wilcox, and M. Rymes. 1993. *Users Manual for SERI QC Software: Assessing the Quality of Solar Radiation Data*. Golden, CO: National Renewable Energy Laboratory. NREL/TP-463-5608. https://www.nrel.gov/docs/legosti/old/5608.pdf.

Michalsky, J. J., M. Kutchenreiter, and C. N. Long. 2017. "Significant Improvements in Pyranometer Nighttime Offsets Using High-Flow DC Ventilation." *Journal of Atmospheric and Oceanic Technology* 34 (6): 1323–32. Accessed September 15, 2021. https://journals.ametsoc.org/view/journals/atot/34/6/jtech-d-16-0224.1.xml.

Osterwald C. R., M. Campanelli, T. Moriarty, K. A. Emery, and R. Williams. 2015. "Temperature-Dependent Spectral Mismatch Corrections." *IEEE Journal of Photovoltaics* 5 (6): 1692–97. https://doi.org/10.1109/JPHOTOV.2015.2459914.

Perez, R., R. Seals, P. Ineichen, R. Stewart, and D. Menicucci. 1987. "A New Simplified Version of the Perez Diffuse Irradiance Model for Tilted Surfaces." *Solar Energy* 39 (3): 221–31.

R. Perez, P. Ineichen, R. Seals, J. Michalsky, Modeling daylight availability and irradiance components from direct and global irradiance, Solar Energy 44, 271–289 , 1990

Reda, I., A. Andreas, A. Habte, P. Gotseff, M. Kutchenreiter, and M. Stoddard. 2019. *NREL Pyrheliometer Comparisons: September 23–October 4, 2019 (NPC-2019)*. Golden, CO: National Renewable Energy Laboratory. NREL/TP-1900-75123. https://www.nrel.gov/docs/fy20osti/75123.pdf.

Reda, I., A. Andreas, P. Gotseff, and M. Kutchenreiter. 2020."Using an Absolute Cavity Pyrgeometer to Validate the Calibration of a Transfer Standard Pyrgeometer Outdoors, Independent from the Reference Value of the Atmospheric Longwave Irradiance." *Atmospheric and Climate Sciences* 10: 530–37.

Reno, M., and C. Hansen. 2016. "Identification of Periods of Clear Sky Irradiance in Time Series of GHI Measurements." *Renewable Energy* 90. https://doi.org/10.1016/j.renene.2015.12.031.

Salis, E., et al. 2019. "Results of Four European Round-Robins on Short-Circuit Current Temperature Coefficient Measurements of Photovoltaic Devices of Different Size." *Solar Energy* 179: 424–36. https://doi.org/10.1016/j.solener.2018.10.051.

Sengupta, M., A. Habte, S. Wilbert, C. Gueymard, and J. Remund. 2021. *Best Practices Handbook for the Collection and Use of Solar Resource Data for Solar Energy Applications*: Third Edition. Golden, CO: National Renewable Energy Laboratory. NREL/TP-5D00-77635. https://www.nrel.gov/docs/fy21osti/77635.pdf.

Sengupta, M., Y. Xie, A. Lopez, A. Habte, G. Maclaurin, and J. Shelby. 2018. The National Solar Radiation Database (NSRDB). *Renewable and Sustainable Energy Reviews* 89: 51–60.

Stamnes, K., S. C. Tsay, W. Wiscombe, and K. Jayaweera. 1988. "Numerically Stable Algorithm for Discrete-Ordinate-Method Radiative Transfer in Multiple Scattering and Emitting Layered Media." *Applied Optics* 27 (12): 2502–09.

Stineman, R. W. 1980. "A Consistently Well-Behaved Method of Interpolation." Creative Computing 6 (7): 54–57.

Stoffel, T., and A. Andreas. 1981. *NREL Solar Radiation Research Laboratory (SRRL): Baseline Measurement System (BMS)*. Golden, CO: Solar Energy Research Institute.

Stoffel, T, and Reda, I. 2009. NREL Pyrheliometer Comparisons: 22 September - 3 October 2008. United States: N. p., doi:10.2172/951020.

Vignola, F., J. Peterson, R. Kessler, V. Sandhu, S. Snider, A. Habte, P. Gotseff, A. Andreas, M. Sengupta, and F. Mavromatakis. 2021. "Improved Field Evaluation of Reference Cells Using Spectral Measurements." *Solar Energy*. https://doi.org/10.1016/j.solener.2020.12.063.

Vignola, F., J. Peterson, R. Kessler, S. Snider, P. Gotseff, M. Sengupta, A. Habte, A. Andreas, and F. Mavromatakis. "Influence of Diffuse and Ground-Reflected Irradiance on the Spectral Modeling of Solar Reference Cells." ASES National Solar Conference Proceedings.

Welch, G., and G. Bishop. 1995. An Introduction to the Kalman Filter (SIGGRAPH 2001 Course 8). Chapel Hill, NC: ACM, Inc.

Wilcox S. M., and D. Myers. 2008. *Evaluation of Radiometers in Full-Time Use at the National Renewable Energy Laboratory Solar Radiation Research Laboratory*. Golden, CO: National Renewable Energy Laboratory. NREL/TP-550-44627.

Xie, Y., and M. Sengupta. 2018. "A Fast All-Sky Radiation Model for Solar Applications with Narrowband Irradiances on Tilted Surfaces (FARMS-NIT): Part I. The Clear-Sky Model." *Solar Energy* 174: 691–702.

Xie, Y., M. Sengupta, and J. Dudhia. 2016. "A Fast All-Sky Radiation Model for Solar Applications (FARMS): Algorithm and Performance Evaluation." *Solar Energy* 135: 435–45.

Xie, Y., M. Sengupta, and M. Dooraghi. 2018. "Assessment of Uncertainty in the Numerical Simulation of Solar Irradiance Over Inclined PV Panels: New Algorithms Using Measurements and Modeling Tools." *Solar Energy* 165: 55–64.

Yoon, H. W., and C. E. Gibson. 2010. *Spectral Irradiance Calibrations*. Gaithersburg, MD: National Institute for Standards and Technology. NIST SP-250-89.

Younkin, K. and C. N. Long. 2003. *Improved Correction of IR Loss in Diffuse Shortwave Measurements: An ARM Valued-Added Product*. Washington, D.C.: U.S. Department of Energy DOE/SC-ARM/TR-009.